AD-A149 272 COBALT-FREE PERMANENT MAGNET ALLOYS(U) COLT INDUSTRIES 1/1
INC PITTSBURGH PA CRUCIBLE RESEARCH CENTER
K S NARASIMHAN ET AL. OCT 84 N00014-81-C-0805
UNCLASSIFIED F/G 11/6 NL

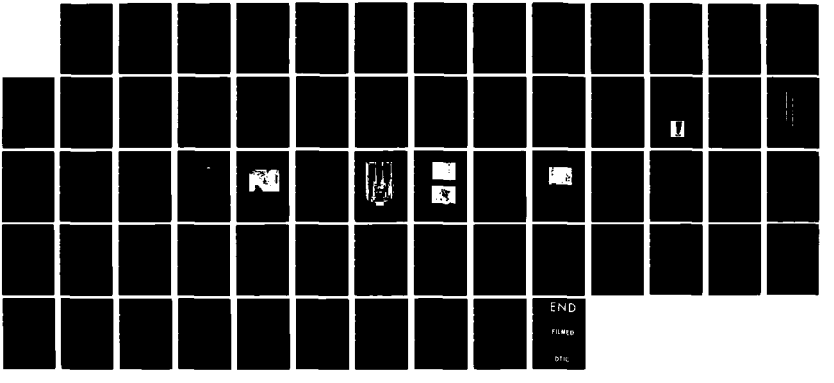

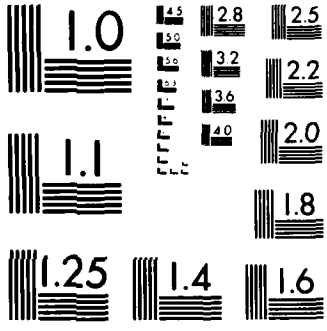

(12)

Office of Naval Research
Contract N00014-81-C-0805

COBALT-FREE PERMANENT MAGNET ALLOYS

by

K. S. V. L. Narasimhan,
Bao-Min Ma
and T. Lizzi

FINAL REPORT

OCTOBER 1984

The research reported in this document was made possible through support by the Office of Naval Research under the above contract.

Colt Industries
Crucible Research Center
P. O. Box 88,
Pittsburgh, Pa. 15230

SECURITY CLASSIFICATION OF THIS PAGE (When Data Entered)

REPORT DOCUMENTATION PAGE	READ INSTRUCTIONS BEFORE COMPLETING FORM
1. REPORT NUMBER	2. GOVT ACCESSION NO. A149272 / 3. RECIPIENT'S CATALOG NUMBER
4. TITLE (and Subtitle) COBALT-FREE PERMANENT MAGNET ALLOYS	5. TYPE OF REPORT & PERIOD COVERED Final Report Oct. 1981 - Dec. 1983
	6. PERFORMING ORG. REPORT NUMBER
7. AUTHOR(s) K. S. V. L. Narasimhan, Bao-Min Ma and T. Lizzi	8. CONTRACT OR GRANT NUMBER(s) N00014-81-C-0805
9. PERFORMING ORGANIZATION NAME AND ADDRESS Colt Industries, Crucible Research Center P. O. Box 88, Pittsburgh, Pa. 15230	10. PROGRAM ELEMENT, PROJECT, TASK AREA & WORK UNIT NUMBERS
11. CONTROLLING OFFICE NAME AND ADDRESS	12. REPORT DATE October 1984
	13. NUMBER OF PAGES 62
14. MONITORING AGENCY NAME & ADDRESS(if different from Controlling Office)	15. SECURITY CLASS. (of this report) Unclassified
	15a. DECLASSIFICATION/DOWNGRADING SCHEDULE

16. DISTRIBUTION STATEMENT (of this Report)

Reproduction in whole or in part is permitted for any purpose by the United States Government.

This document has been approved for public release and sale; its distribution is unlimited.

17. DISTRIBUTION STATEMENT (of the abstract entered in Block 20, if different from Report)

18. SUPPLEMENTARY NOTES

19. KEY WORDS (Continue on reverse side if necessary and identify by block number)

20. ABSTRACT (Continue on reverse side if necessary and identify by block number)

We have undertaken the study of cobalt-free alloys for evaluation of their use in permanent magnet fabrication. A two-phase study was carried out. In the first phase, the plasma arc process was employed for the production of fine powder of MnAlC and the second phase was confined mainly with melt spinning. Both these rapid solidification technology approaches should permit stabilization of metastable phases and offer a unique technique of generating coercivity.

DD FORM 1 JAN 73 1473 EDITION OF 1 NOV 65 IS OBSOLETE

SECURITY CLASSIFICATION OF THIS PAGE (When Data Entered)

20. Abstract (Concluded)

The results of our investigation indicate that melt spinning of boron containing Nd-Fe and Pr-Fe alloys can provide high values of coercive force and saturation magnetization. The composition of the magnetic phase responsible for the high coercive force was identified to be $R_3Fe_{20}B$.

ACKNOWLEDGEMENTS

We are thankful to Dr. Donald E. Polk, Office of Naval Research Monitor for the program, for several fruitful discussions. The work was actively supported by the entire CRC staff, in particular our President, E. J. Dulis.

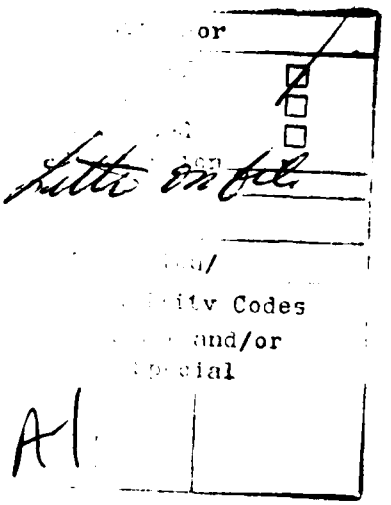

TABLE OF CONTENTS

LIST OF ILLUSTRATIONS

LIST OF ILLUSTRATIONS (CONCLUDED)

LIST OF TABLES

SECTION 1

INTRODUCTION

The critical raw material cobalt for decades maintained a relatively stable price pattern until 1978 when the price jumped nearly 8 fold. Figure 1 shows the price increase in cobalt relative to the value in 1972. The dramatic increase of 1978 has now slowed down and the price level is now about five fold from that in 1972, but the continual threat of repetition of the events of 1978 always exists and the supply could be interrupted altogether.

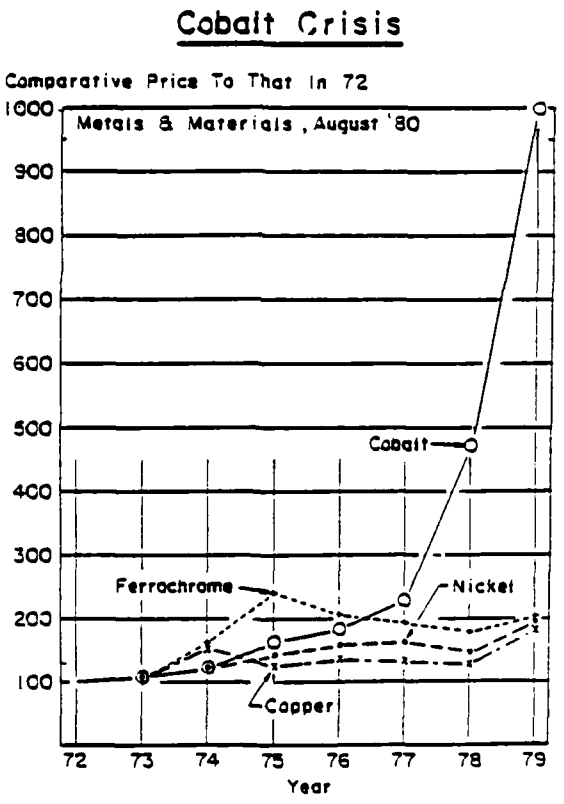

Figure 1. Cobalt Crisis.

The most important sources of refined cobalt production are in order[1]: Zaire, USSR, Zambia, Japan, Finland, France, United Kingdom, Norway, and Canada.

Of the total world production, the major amount of cobalt is imported from Zaire. Figure 2 shows the extent of cobalt production at Zaire compared to the total world production. The U. S. imports nearly 75% of its cobalt from South Africa (Zaire, Zambia, Botswana, and the republic of South Africa). Although there is an adequate amount of cobalt in the world, the reliance of U. S. for cobalt on highly unstable countries makes it necessary for us to decrease the dependence on cobalt.

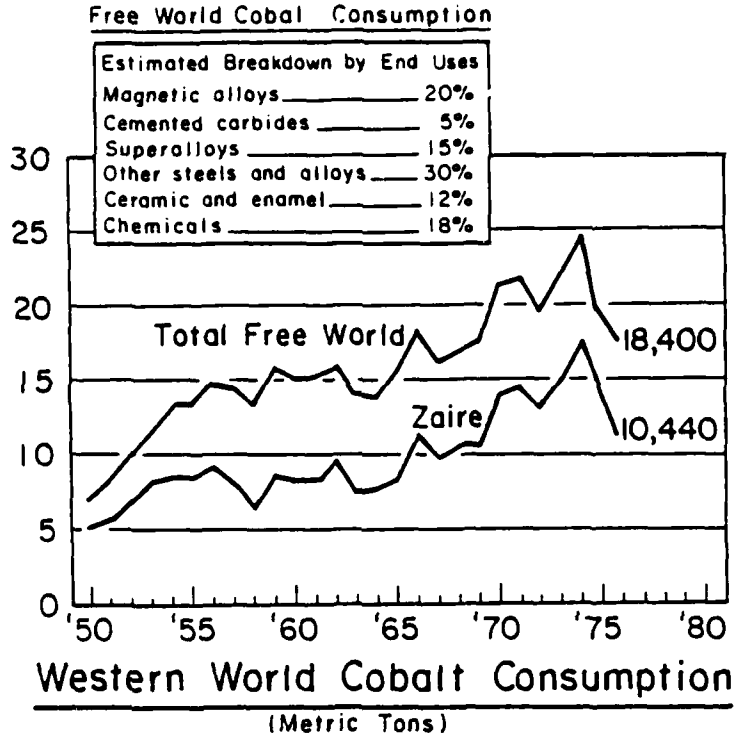

Figure 2. Free World Cobalt Consumption.

Table 1 provides a list of critical raw materials and U. S. dependence on foreign sources.

TABLE 1

THE PERCENTAGE DEPENDENCE ON FOREIGN SOURCES FOR CRITICAL RAW MATERIALS

METAL	DEPENDENCY %	SOURCES
CHROMIUM	90	SOUTH AFRICA, USSR
TITANIUM	100	AUSTRALIA, JAPAN
COBALT	90	ZAIRE, ZAMBIA
COLUMBIUM	100	BRAZIL, CANADA
TANTALUM	96	THAILAND, CAN

Of the critical raw materials that are imported, cobalt supply is dependent on politically unstable countries.

Figure 2 shows the consumption of cobalt by industry segments. Permanent magnets and superalloys consume over one-third the cobalt imported. Alternate magnet materials that do not contain cobalt can relieve foreign dependence. Alnico-5 permanent magnets which contain 24% cobalt are a major consumer of cobalt. The magnetic properties of these magnets are B_r (induction) = 12,500G, H_c(coercivity) = 6400e, BH_{max} (energy product) = 5.5MGOe. They have a low reversible temperature coefficient. To replace Alnico-5, one can use a ferrite which contains no cobalt but the magnet sizes have to be large because of the lower load line under which ferrites operate. This results in a bulky device. A major further disadvantage of ferrite is its high temperature coefficient, i.e., substantial loss of induction at moderately high temperatures.

Rare-earth cobalt magnets with an energy product nearly four times that of Alnico-5 contain ∿65% cobalt but can replace Alnico-5 with an overall reduction in the cobalt content because the higher energy product of the rare-earth cobalt magnets results in the use of a smaller volume of the magnet. Yet a substantial cobalt requirement remains.

Hence, a need exists for a cobalt-free permanent magnet to be developed which has properties between those of Alnico-5 and rare-earth cobalt. Such a magnet will make it possible for designers to switch from the currently used Alnico-5 or rare-earth cobalt with the least amount of difficulty. A major application of permanent magnets is in motors.

A program plan to achieve the goal of obtaining a non-cobalt containing permanent magnet with a remanence between 6,000 - 10,000 Gauss and a coercive force of 1,000 - 3,000 Oersteds was undertaken.

SECTION 2

TECHNICAL DISCUSSION

Criteria for Permanent Magnet

Permanent magnet materials have the ability to retain the magnetized condition for indefinite length of time. The ability of a magnet to withstand demagnetizing field is dependent on the origin of the magnetic anisotropy of the material constituting the magnet. If the anisotropy arises from the shape, then the magnet material cannot withstand high demagnetizing fields in open circuit-conditions whereas if the anisotropy is crystalline in origin then a larger demagnetizing field can be imposed on the magnet. There are other methods of inducing an anisotropy such as straining the material but the coercive force generated by this method is inferior to that of both shape and crystal anisotropy.

TABLE 2

COERCIVE FORCE - GENERATION

To Generate Coercive Force Of 810 Oe		
	Strain Induced	
340,000 lb./in.^{2}	$H_{ci} \propto \lambda \frac{Z}{M_s}$	λ = Magneto Striction Constant Z = Internal Strain M_s = Saturation Magnetization
	Shape Induced Anisotropy	
$\frac{c}{a} = 1.1$	$H_{ci} \propto (N_B - N_A) M_s$	
	N_B and N_A are the demagnetization factors along the major and minor axes.	
	Crystalline Anisotropy	
$K = 7 \times 10^5$ erg/cm^3	$H_{ci} \propto \frac{K}{M_s}$	
($M_s = 1714$ emu/cm^3, $\lambda = 20 \times 10^{-6}$)	K = Anisotropy Constant	

Table 2 provides the common methods of generating the coercive force. The table also shows the amount of strain or distortion of shape or crystalline anisotropy that is required to generate a coercive force of 810 Oe. Crystal anisotropy which is intrinsic to the material is far the most effective method of generating the coercive force but not all the materials have the desired magnetocrystalline anisotropy and hence shape anisotropy offers a next best method of achieving the coercive force. Table 3 lists some of the currently available permanent magnet materials and the origin of anisotropy in these materials.

TABLE 3

ORIGIN OF ANISOTROPY AND MAGNETIC PROPERTIES OF SOME PERMANENT MAGNET MATERIALS

Alloy	Remanence (Br) G	Coercive Force (H_c) Oe	Energy Product (BH_{max}) MGOe	Origin of Anisotropy
Alnico	12,600 10,500 13,500	665 1,600 740	5.5 9.0 7.5	Shape
FeCrCo	13,500 14,500	600 700	6.0 7.5	Shape
Vicalloy	11,000	300	1.7	Strain
$ReCo_5$	10,000 10,600	9,000 10,600	25-28	Crystal
Ferrite	4,100 4,300	2,900 2,500	4-4.2	Crystal

In order to develop a permanent magnet shape or crystal, anisotropy should be present in the magnetic alloy.

The temperature of operation of permanent magnets extend up to 100°C and, in some cases, up to 200°C. This would necessitate the magnet alloy to have a Curie temperature above 200°C preferably up to 300°C. The higher the Curie temperature the better is the temperature dependence of magnetic flux.

The attainment of high Curie temperature is dependent on the strength of exchange field or the internal Weiss-molecular field which is in turn controlled by the atomic arrangements and the electronic structure. In general, alloys containing Fe, Co, Ni or Mn have high Curie temperatures.

The energy product of a magnet, BH_{max}, controls the total volume of the magnetic material required for a specific application. The saturation induction of a magnetic alloy controls the maximum value of B that can be obtained in a magnetic alloy. The higher this value the better is the energy product. Alloys containing Fe, Co, or Mn have high saturation induction.

The requirements for an alloy to be useful as a permanent magnet can be summarized as follows:

1. Curie temperature of the alloy be above room temperature.
2. Reasonable saturation magnetization.
3. The alloy possess either crystal anisotropy or is able to be processed to single domain elongated particles. This requirement provides the coercive force.
4. The alloy to be investigated in this proposal should not contain cobalt.

The second requirement limits the alloy systems to those with a saturation magnetization greater than 60 emu/gm.

The third requirement of crystalline shape anisotropy is most crucial as this will determine the coercive force. Special powder production techniques have to be employed to minimize crystal distortion which otherwise will reduce both coercive force and remanence. Special powder processing techniques may be required to impart coercive force in a system that does not have crystal or easily attainable shape anisotropy.

Alloy Selection

With the objective of developing magnet alloys that do not contain cobalt and which have the requirements as set forth in the previous section, an examination of the literature indicates several alloys to have a potential to be a permanent magnet. We will confine our discussion to the following alloys:

1. (Fe-B) with rare earth additions
2. Rare earth-iron alloys
3. MnAlC system

(Fe-B) with Rare Earth Addition

Fe-B alloy in the stoichiometry $Fe_{0.82}B_{0.18}$ shown unusual magnetic and physical characteristics that is of importance in soft magnetic material applications. However, Koon et al[2] have shown that this alloy can be suitably modified by rare earth substitution to produce hard magnetic material. The approach these authors have taken is to first obtain an amorphous film of the alloy under investigation and later crystallize the alloy with or without the presence of magnetic field. During recrystallization, nearly single domain particles are obtained resulting in high coercive force.

The addition of heavy rare earth such as Tb to $Fe_{0.82}B_{0.18}$ would normally result in the formation of binary alloy of $TbFe_2$ and preventing the formation of amorphous alloy (Fe-B) containing Tb. The discovering of Koon et al that the addition of La prevents such an alloy formation made it possible for the preparation of $(Fe_{0.82}B_{0.18})_{0.9}Tb_{.05}La_{.05}$ in the amorphous state. This alloy when recrystallized produced a B_r=4,800 Gauss and intrinsic coercive force (H_{ci}) of 10,000 Oe at room temperature.

The attractive values of the coercive force obtained by Tb and La substitution suggest that further investigation with other rare earth preferably the light and some of the heavy rare earth have a potential to achieve the currently proposed program goals.

The mechanism of obtaining the coercive in the present program is discussed later. The proposed mechanism will have the added advantage of producing much higher remanence.

Rare Earth-Iron System

The discovery of hard magnetic properties[3] in the recrystallized amorphous film of $SmFe_2$, $TbFe_2$ and $DyFe_2$ indicated that these Laves phase alloys, although cubic, do possess a unique axis of magnetization that permits the realization of high coercive force.

The RFe_2 composition has the highest Curie temperature among the various intermetallics that can be formed from the RFe series. Thus the RFe_2 alloys are attractive candidates for the development of permanent magnets.

A detailed discussion of the various phases that are present in RFe series is given by J. Schweizer[4] and Buschow[5]. Under normal processing conditions, alloys from Sm-Lu exist with RFe_2 stoichiometry. $LaFe_2$, $PrFe_2$ and $NdFe_2$ are difficult to form. Table 4 lists the Curie temperatures and the easy direction of magnetization for the various binary RFe alloys[5,6]. From this table, it is seen that quite a few alloy systems exist with a Curie temperature close to 300°C. The selection of a particular alloy would depend on its saturation induction at the useful temperature range and the cost of the raw material. Yttrium alloys offer a good promise but certain amounts of Sm, Pr, Nd, or heavy rare-earths may be necessary to impart a unique axis of magnetization which in turn will benefit the attainment of coercive force.

TABLE 4

ALLOY SYSTEMS, CURIE TEMPERATURE AND EASY DIRECTION OF MAGNETIZATION IN THE R-Fe BINARY

Alloy System	Curie Temperature	Easy Direction of Magnetization (a unique axis of magnetization is prefered for a good magnet)
$CeFe_2$	- 68°C	(100) L.T.
$SmFe_2$	415°C	(101) L.T.
$GdFe_2$	523°C	(100) L.T.
$TbFe_2$	431°C	(111) L.T.
$DyFe_2$	362°C	(100) R.T.
$HoFe_2$	335°C	(100) L.T.
$ErFe_2$*	314°C	(111) R.T.
$TmFe_2$*	326°C	(111) L.T.
YFe_2	269°C	(111) L.T.
$SmFe_3$	377°C	c - axis (L.T.)
$GdFe_3$	456°C	basal plane (R.T.)
$TbFe_3$	379°C	b - axis (L.T.)
$DyFe_3$	333°C	b - axis (R.T.)
$HoFe_3$	298°C	b - axis (R.T.)
$ErFe_3$*	279°C	b - axis (R.T.)
YFe_3	296°C	b - axis (L.T.)
Gd_6Fe_{23}	386°C	N.A.
Tb_6Fe_{23}*	301°C	N.A.
Dy_6Fe_{23}*	261°C	N.A.
Ho_6Fe_{23}*	257°C	(111) (L.T.)
Er_6Fe_{23}	221°C	(111) (L.T.)
Tm_6Fe_{23}	202°C	N.A.
Y_6Fe_{23}	208°C	(100) (L.T.)
Ce_2Fe_{17}	- 35°C	-
Pr_2Fe_{17}	10°C	b - axis (L.T.)
Nd_2Fe_{17}	56°C	a - axis (L.T.)
Sm_2Fe_{17}	95°C	N.A.
Gd_2Fe_{17}	203°C	ab plane (L.T.)
Tb_2Fe_{17}	135°C	a - axis (L.T.)
Dy_2Fe_{17}	98°C	b - axis (L.T.)
Ho_2Fe_{17}	52°C	a - axis (L.T.)
Er_2Fe_{17}	32°C	b - axis (L.T.)
Tm_2Fe_{17}	7°C	c - axis (L.T.)
Y_2Fe_{17}	51°C	b - axis (L.T.)

*These alloy systems are unsuitable because of the compensation temperature close to room temperature resulting in lower saturation magnetization.

L.T. = at low temperature, R.T. = at room temperature
N.A. = not available

R_2Fe_{17} alloy systems have the highest saturation at room temperature but unfortunately with low Curie temperature. Narasimhan et al[7] have shown that small amounts of nickel substitution can increase the Curie temperature dramatically (see Figure 3). Investigation of Ni containing R_2Fe_{17} alloy show promise for further investigation.

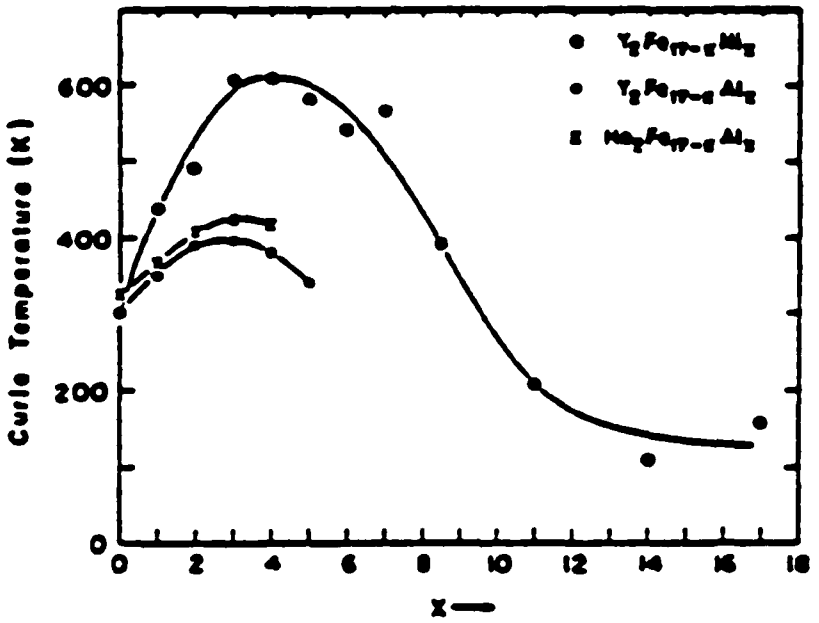

Figure 3. Increase in Curie Temperature in the Nickel Substituted Y_2Fe_{17} Alloys.

Pr-Fe system have shown high intrinsic coercive force when an amorphous film of this alloy is recrystallized[8]. Further improvement in the coercive force and the saturation induction is necessary. Substitution of Sm for Pr and heavy rare-earths with an objective of increasing saturation has to be investigated.

MnAlC System

MnAlC with a body centered tetragonal structure has an easy C-direction of magnetization with an anisotropy field of 40 kOe and a maximum theoretical potential of 16 MGOe.

The current method of making MnAlC anisotropic magnet is to warm extrude the alloy to bring forth grain orientation along the C-axis. The extent of orientation achieved is normally about 70% and hence to achieve full potential, techniques other than warm extrusion have to be explored.

The primary magnetic properties of MnAlC suggest that it should be possible to crush MnAlC close to single domain particle size, orient in a magnetic field, press and sinter. A calculation based on the available data on MnAl suggest a single domain particle size to be 0.4μ.

A processing technique that would produce 0.4μ or less MnAl powder has an advantage of directly producing single domain particles. Conventional crushing techniques result in the deformation of crystal lattice resulting in poor magnetic quality. There is an additional advantage of the use of 0.4μ powder and that is in the phase transformation process.

MnAl magnetic tetragonal phase (τ) is formed from the non-magnetic high temperature hexagonal ε phase via martensitic transformation. During this transformation, a ε crystal transforms to six τ orientations to accommodate the distortions that occur during the transformation.

The use of ultra fine powder of ε will result in only a single τ orientation crystal, since the ε grains are small. The use of fine powder has a similar effect as extrusion in the sense that during extrusion stress are exerted to direct the orientation of ε grains to τ phase of nearly single orientation.

Generation of Coercive Force

The generation of coercive force in the above systems will be achieved by preparing nearly single domain particles as opposed to milling a cast alloy to produce fine particles for compaction in a magnetic field.

This approach is necessary because the single domain particle radius for $DyFe_2$ (which has an anisotropy constant of $2X10^7$ erg/cm^3) is 0.8 and for other alloy systems such as MnAlC it is 0.4μ. To achieve this particle size by milling will result in the introduction of lattice defects that will lower the saturation magnetization as well as the coercive force.

Additional advantage of producing fine powder by the rapid solidification technology is the ability to produce metastable phases which in normal slow cooling of mold castings will decompose to more stable phases.

Methods for the preparation of ultra fine powders that will contain the fewest defects have to be developed.

SECTION 3

PROGRAM PLAN

The program plan was divided into two phases:

Phase I - Examination of the Feasibility of Plasma Arc Process for Powder Production.

Phase II - Examination of Processes for Rapid Solidification.

The alloys to be studied in the program were:

MnAlC
Rare Earth-Iron Alloys

SECTION 4

PHASE I - PLASMA ARC PROCESS

Columbia University had developed a unique plasma arc process for the generation of fine powders in the submicron range and this is referred to as the Sheer-Korman Process. The "fluid convection cathode" (FCC) is a new technique of generating the plasma and is an effective method for vaporizing powder particles.

The principle of the method is illustrated in Figure 4.

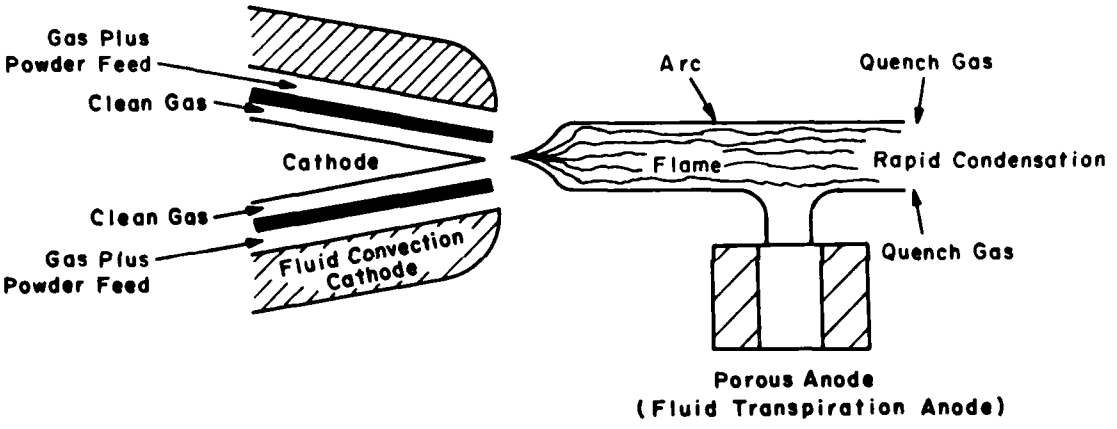

Figure 4. Fluid Convection Cathode set-up used for powder production.

The powder to be vaporized is fed along with the gas stream near the cathode and the stream is directed towards the hottest area of the plasma referred to as plasma bubble. The plasma bubble is from the differences in current density a little distance away resulting in changes in the magnetic field which then attracts the plasma into this area forming a bubble. The plasma bubble (see Figure 5) permits vaporization of the powder along the length of the arc column.

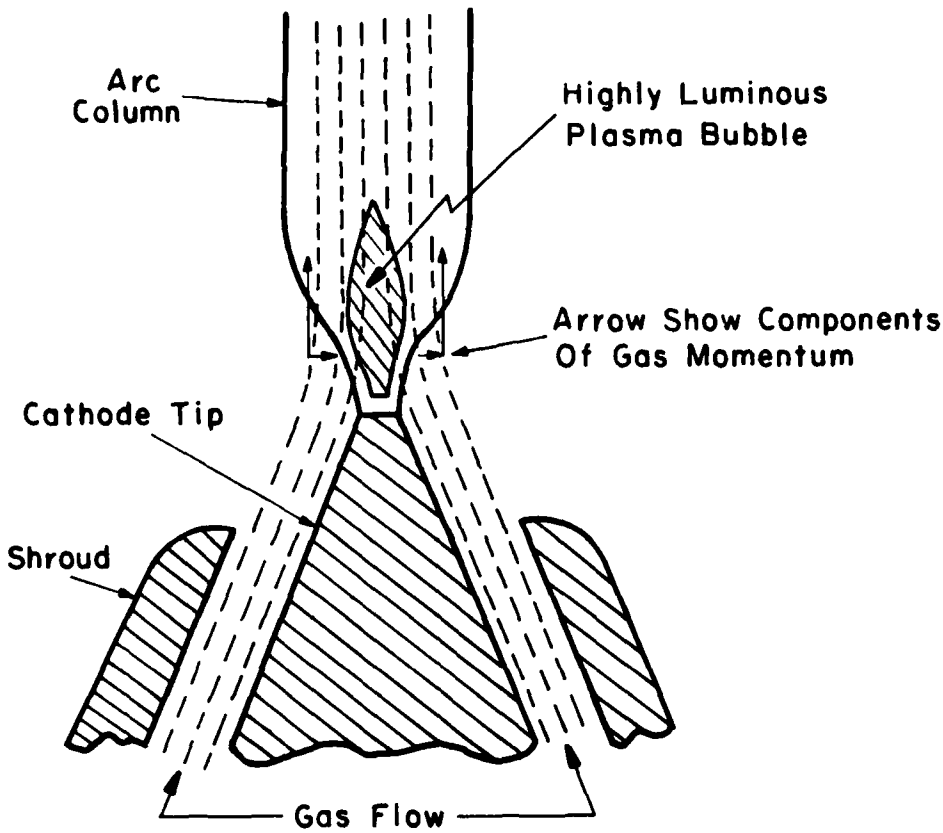

Figure 5. Sketch of fluid convection cathode nozzle.

The arc column is shown in Figure 6.

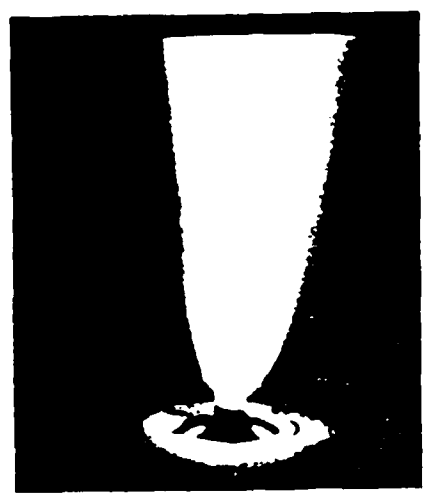

Figure 6. Arc column in the Sheer-Korman process.

The temperature attainable by this arc process is 15,000°F. In a typical run, 70-80% of the feed is vaporized and the feed particle size can be as coarse as -60 mesh.

Table 5 illustrates the typical materials that were vaporized by the plasma arc process by Professors Sheer and Korman.

TABLE 5

SUBMICRON MATERIALS PRODUCED USING THE HIGH INTENSITY ARC PROCESS

Oxides	Metals	Carbides	Multicomponent systems	
SiO_2	C	ThC	Ferrites	(Zn, Mn, Cu, Fe)O
Al_2O_3	Al	TiC	Kaolin	$Al_2O_3 \cdot SiO_2 \cdot Fe_2O_3$
Fe_2O_3	Li	B_4C	Spodumene	$LiAl(SiO_3)_2$
ThO_2	Ni	UC	Rhodonite	$MnO \cdot SiO_2$
MnO_2	Fe	TaC	Ferrosilicon	$Fe \cdot Si$
Cb_2O_5	W	SiC	Chromite	$FeO \cdot Cr_2O_3$
NiO	Mo		Euxenite	$Y_2Er_2Ce_2U_2(Ta,Cb)_4O_{15} \cdot xH_2O$
Y_2O_3			Boron carbide · silicon carbide	$B_4C \cdot SiC$
UO_2			Uranium carbide · columbium carbide	$UC \cdot CbC$
MoO_3			Uranium carbide · thorium carbide	$UC \cdot 2 \cdot 25ThC$
ZrO_2				
MgO				
WO_3				

Use of this Process for MnAlC

As indicated in the Introduction, it was necessary to produce MnAlC in the 0.4 micron size and rare earth-iron to 0.8 micron size. We undertook the study of MnAlC initially as it has less expensive raw materials than the rare earth-iron and thus provides a method of evaluating the applicability of the process for magnetic materials.

The powder of submicron size will oxidize when exposed to air and hence a special container set-up (see Figure 7) was used for collecting the powder from the plasma arc process.

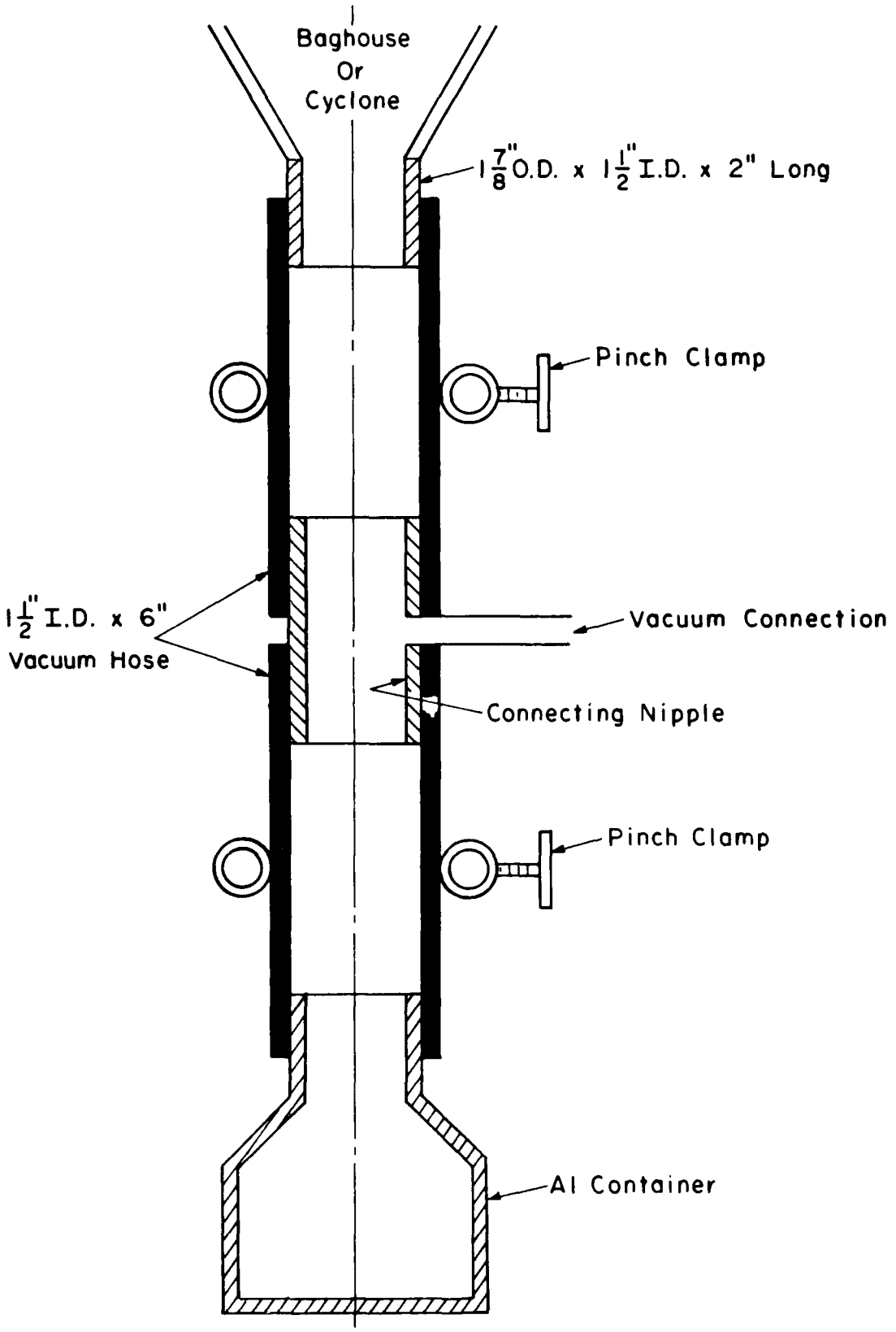

Figure 7. Collector can for powder produced in the plasma arc process.

The sealed cans were opened in an inert gas atmosphere, loaded into various containers for magnetic evaluation.

The powder obtained from Columbia University has to be transformed to the magnetic T phase from the non-magnetic ε phase. We have used powder produced by conventional methods to study the transformation kinetics. Powder of MnAlC of the same composition used for plasma spraying was heated to temperatures ranging from 800°F to 1500°F from 15 minutes to 1 hour. Figure 8 shows the temperature dependence of the ε to T transformation.

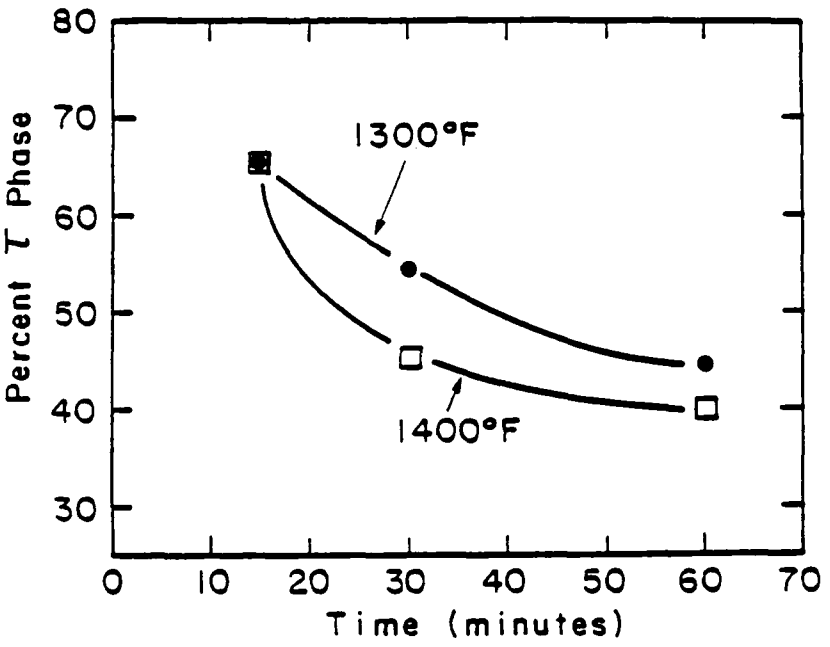

Figure 8. Effect of time on the amount of T phase formed in isothermal transformations.

Figure 9 shows the transformation process for one hour hold at various temperatures. As can be seen, the transformation is maximum at 1000°F for an hour hold. We had used magnetization data to indicate the extent of transformation.

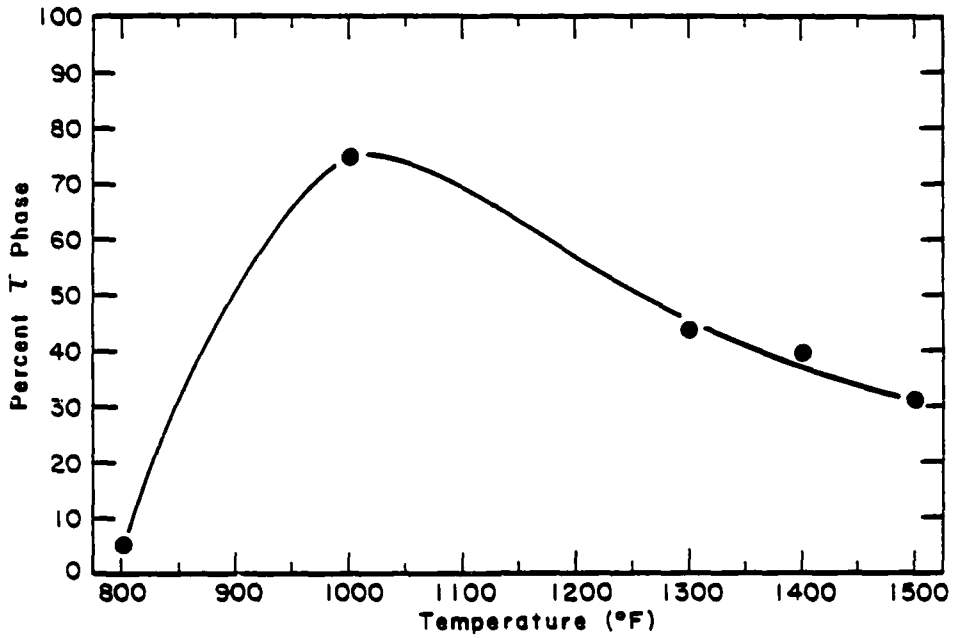

Figure 9. Isothermal transformation of ε phase to T phase for one hour hold at temperature.

The as-received powder from Columbia University was non-magnetic as expected since the high temperature ε phase is formed during the plasma arc process. This powder was loaded into a copper tube and heat treated at 1000°F for 45 minutes. X-ray diffraction pattern indicated the presence of magnetic T phase. Hysteresis loop was measured on the heat treated powder dispersed in wax. The results were as follows:

Sample	Heat Treatment	B_r (G)	H_{ci} (Oe)
MnAlC (T phase) (70%Mn, 28.7%Al, 0.5C, 0.8 Ni)	1000°F - 45 minutes	2,100	1,600

The first quadrant indicated lack of saturation even at 20 kOe. The $4\pi M_s$ measured at 20 kOe was 4,600 Gauss.

The above results are compared in Table 6 with the best coercive force achieved on -45 mesh powder, ball milled 5 micron powder and as-cast alloy heat treated.

TABLE 6

INTRINSIC COERCIVE FORCE OF MnAlC

Method of Powder Production	H_{ci} (Oe)
-400 micron mesh powder from vacuum cast alloy, heat treated	720
Ball milled 5 micron powder, heat treated	400
Arc plasma produced powder, heat treated	1,600
As-cast alloy, heat treated	1,200

The results obtained indicate that arc plasma powder, although produced the highest H_{ci}, the H_{ci} values are far below that obtained on a warm extruded alloy (∿5000 Oe). The origin of the coercive force is perhaps from defects introduced during the warm extrusion process which helps in pinning the domain walls and the powder technique does not provide the defects.

Additional work involving the introduction of defects in the powder may be necessary to permit the realization of the powder technique of making MnAlC magnets.

PHASE II - RAPID SOLIDIFICATION TECHNIQUES

Metastable phases of rare earth-iron can be produced by rapid solidification. The technique of achieving rapid solidification is wide and varied. We had used two techniques for rapid solidification: plasma spray approach and melt spinning approach.

Plasma Spray Approach

Plasma spraying permits powder of the alloy of interest to be melted and sprayed with an instant cooling of the powder. A schematic of the Metco 2MB plasma gun is shown in Figure 10.

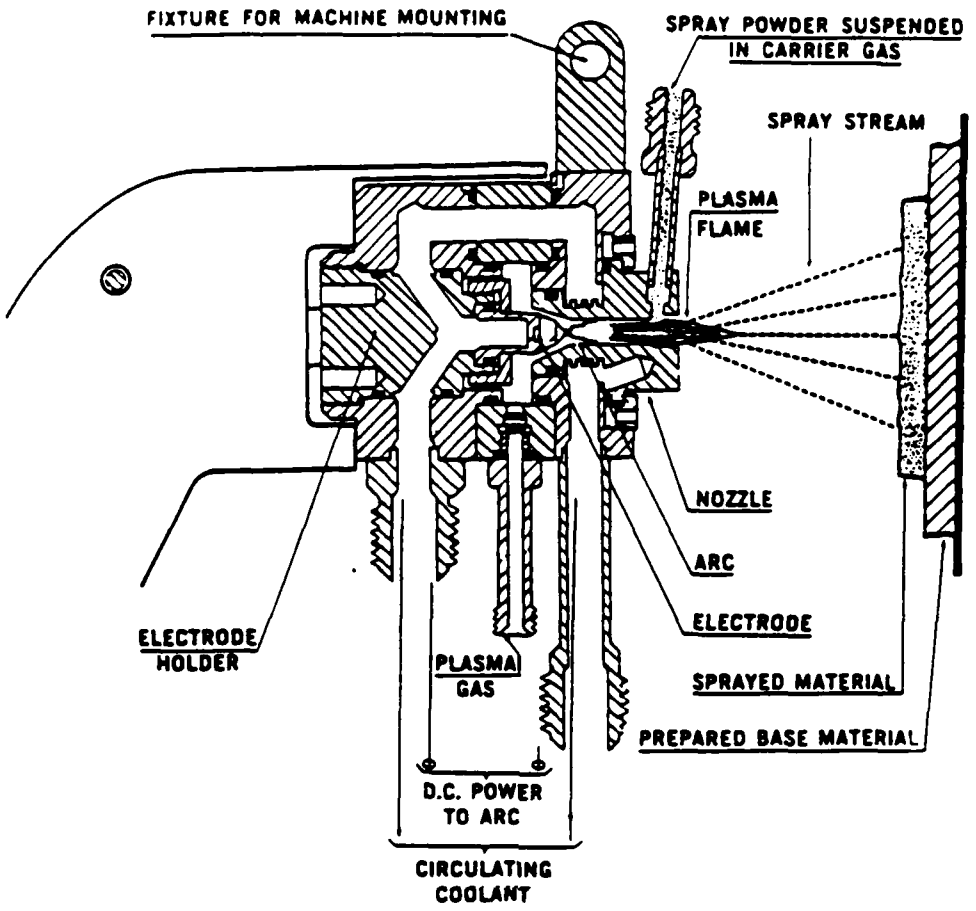

Figure 10. Metco type 2MB plasma flame spray gun cross section.

Powder particles entrained in a carrier gas are introduced into the plasma flame near the front of the gun. The high temperature of the plasma melts the particles and the surface tension makes these melted particles form a sphere. The high pressure gas on exiting the gun undergoes an expansion resulting in cooling of the particle.

The Metco 2MB plasma spraying system consisting of a power supply, control board, powder feeder and plasma gun. The plasma gun was mounted inside a large vacuum chamber (∿40 inches diameter by six feet long). Provisions were made to the chamber to exhaust the gas used during plasma spraying.

An interlock was also added to the chamber. A stainless steel collector drum (24 inches diameter by 30 inches deep) was fabricated to collect the plasma sprayed powder. The powder and gasses from the plasma gun enter the drum through a six inch diameter aperture in the center of the cover for the drum. The gasses exit through a nine inch diameter opening in the side of the drum (see Figure 11).

Figure 11. Plasma spraying laboratory showing the control panel (left), powder feeder (background), vacuum/inert gas chamber (center), and the powder collector drum (foreground).

At the beginning of a plasma spraying trial, the powder to be sprayed is placed into the hopper of the powder feeder. The powder feeder is outside of the vacuum chamber. The hopper is gas tight and connected to the plasma gun by a quarter inch diameter polyflo hose through which the powder, entrained in a carrier gas (He), is fed into the plasma gun.

Once the powder is in the hopper and the hopper has been sealed, the vacuum chamber and hopper are pumped down to a vacuum of about 40 μm. The system is then backfilled with argon. The oxygen level is measured to be typically below 50 ppm (see Figure 12).

At start up the gas flow through the plasma gun is initiated and the electric power gradually increased to about 25 kw. The powder feeder is then activated. The powder feed rate is kept low (∿10 g/min.) to promote particle melting. A great deal of heat is evolved by the plasma spraying process and this causes the weld chamber to heat up quickly. To prevent failure of the rubber gloves and seals on the vacuum chamber, the plasma spraying system is shut down after about fifteen minutes of operation.

After the weld chamber has sufficiently cooled, the plasma sprayed powder is removed and examined by SEM for particle morphology and chemical composition.

$PrFe_2$ has been reported to exist as a metastable phase. This alloy was prepared by vacuum melting and prepared in powder form to feed into the plasma gun. It was anticipated that plasma sprayed powder would produce amorphous alloy which then can be recrystallized to produce a fine grain structure.

The plasma sprayed powder of PrFe is shown in Figure 13. As can be seen, a certain amount of spheroidization did occur during plasma spraying. X-ray analysis indicated that powder produced is crystalline.

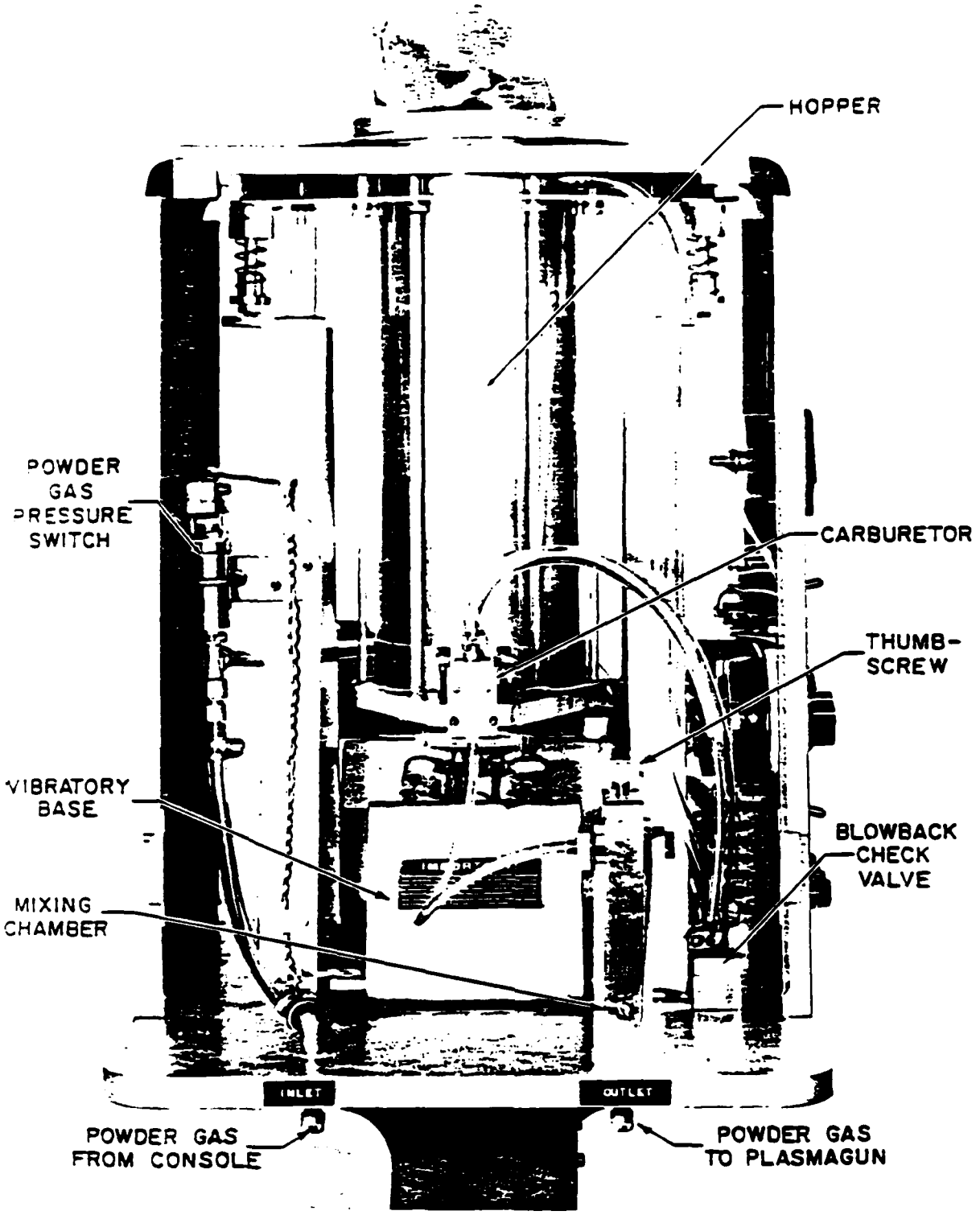

824-84

Figure 12. Metco Model PF-200 powder feeder unit. The control panel is on the right side. The unit also has a screw feed which is not shown here.

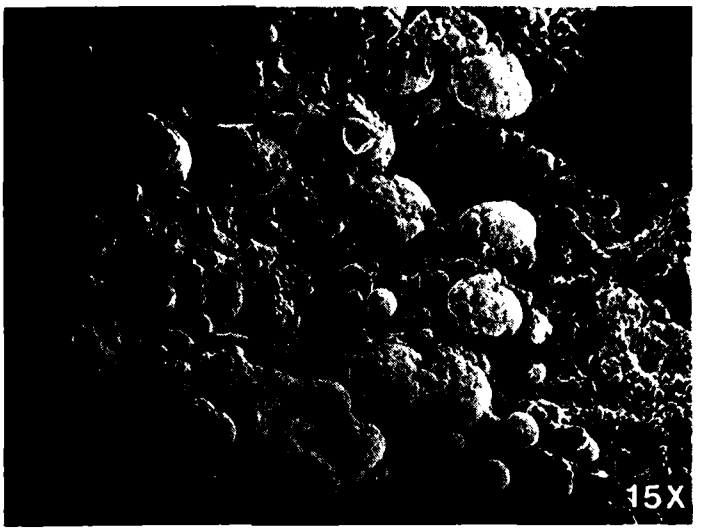

822-84

(a)

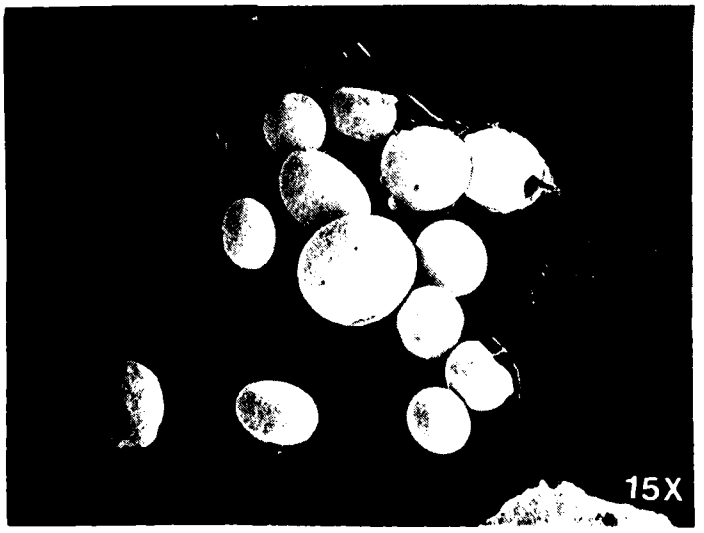

823-84

(b)

Figure 13. Plasma sprayed powder of Pr-Fe showing partial melting (a) and spheroidization (b).

Melt Spinning

Melt spinning of rare earth-iron alloys was attempted with a view of achieving extremely rapid quenching. The technique employed is similar to planar flow casting. In this process (see Figure 14), molten metal of the desired alloy is dropped on to a rotating chilled copper wheel. This permits heat extraction at a rate of a million degrees per second. The entire casting operation is carried out in a glove box. A constant wheel speed of 2,800 feet per sec. (14 meter/sec.) was employed.

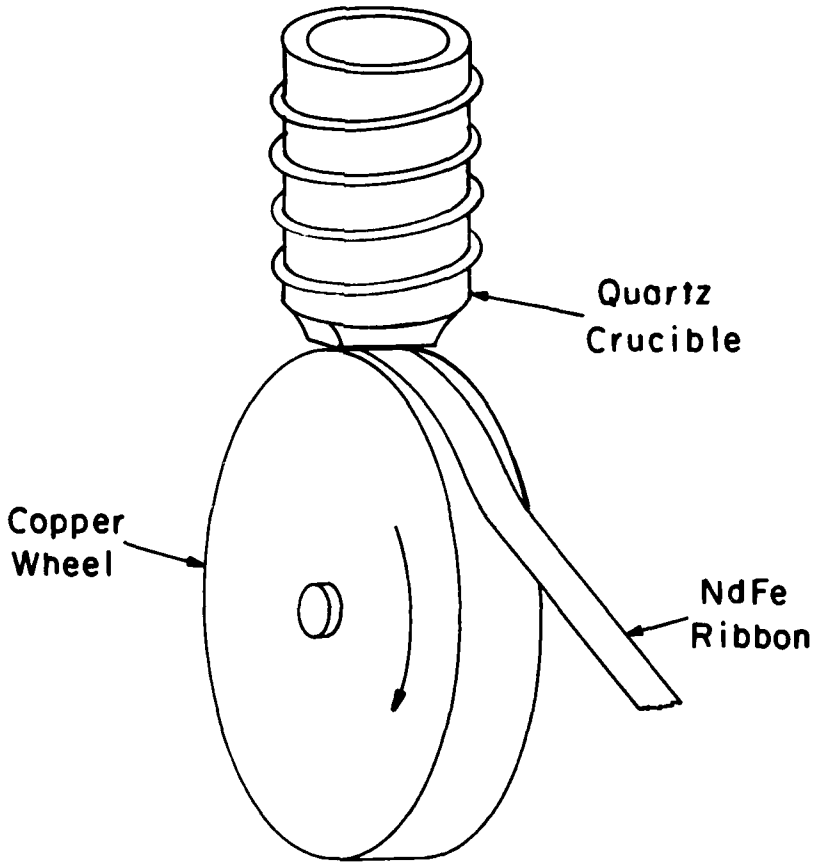

Figure 14. Planar flow casting type of process for melt spinning (Courtesy of M. C. Narasimhan, STAM).

Typical ribbons produced by this process are shown in Figure 15. X-ray diffraction of the ribbons indicated that it is possible to obtain an amorphous structure.

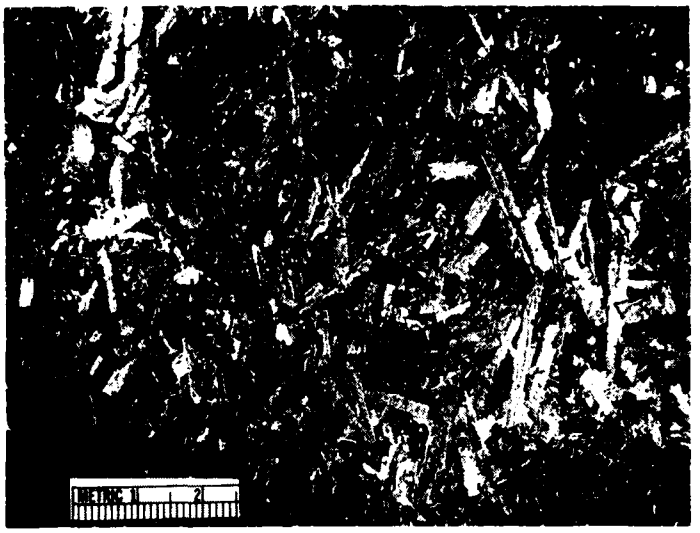

821-84

Figure 15. Typical ribbons produced by the melt spin process.

All subsequent work was carried out using melt spun alloys. The research in the melt spun alloys can be classified into four categories:

1. Alloys of Pr with Fe
2. Alloys of Nd with Fe
3. Alloys of Sm with Fe
4. New magnetic material with high potential.

Pr-Fe Alloys

Magnetization (M) versus temperature (T) data on the rapidly quenched $PrFe_2$ alloy indicated that there are three magnetic phases with a T_c of 21°C, 227°C and a broad peak at 575°C. In order to interpret the T_c data, it is important to recognize the T of the various binary phases.

Figure 16 is a plot of the T_c of various rare earth-iron binary alloys.

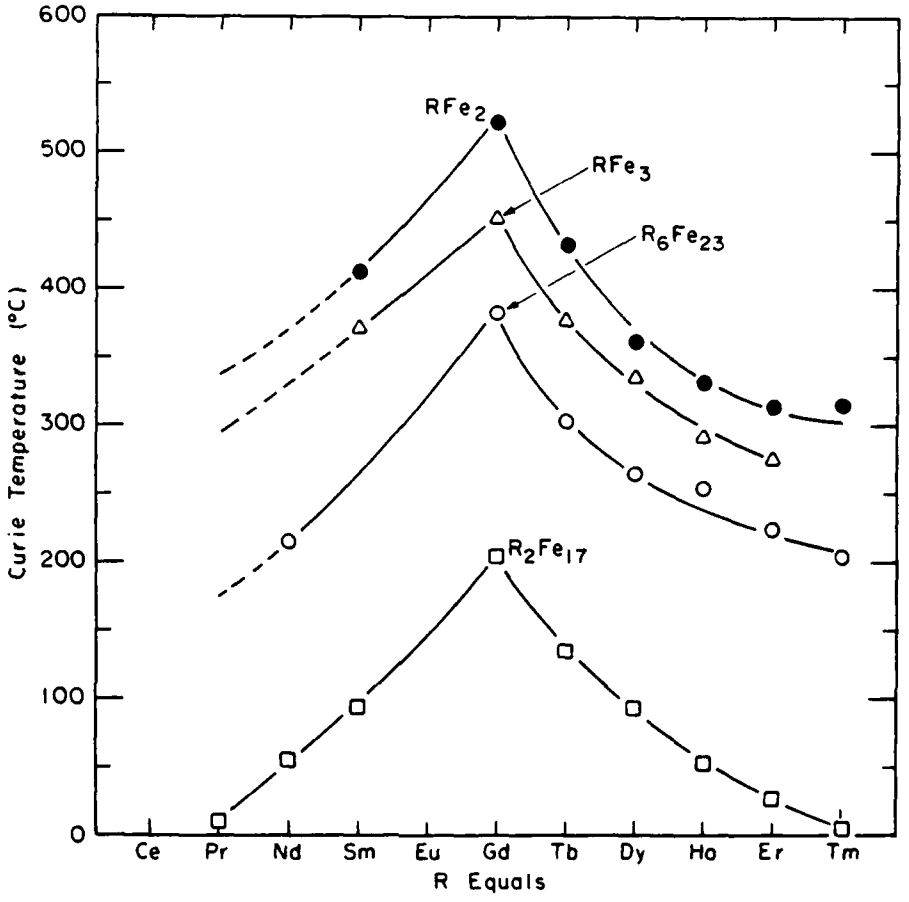

Figure 16. Curie temperature variation of various binary rare earth-iron alloys with the rare earth partner.

Using Figure 16, we can interpret that the rapidly quenched $PrFe_2$ contains 2:17 phase with a T_c of 21°C, a 6:23 phase with a T_c of 227°C. The broad peak at 575°C is interpreted as due to the crystallization of the amorphous component in the alloy (we have noted that in some of the boron-containing melt spun alloy there is a correlation between the crystallization of the amorphous phase as determined by X-ray diffraction with that of the broad peak observed in the magnetization versus temperature data).

The coercivity of the as melt spun alloy was 1300 Oe.

The presence of 6:23 phase instead of 1:2 phase was believed to be due to the oxidation of Pr during alloy making and processing. Hence an alloy richer in Pr was made. The M vs T data are shown in Figure 17 for $PrFe_{1.5}$ alloy.

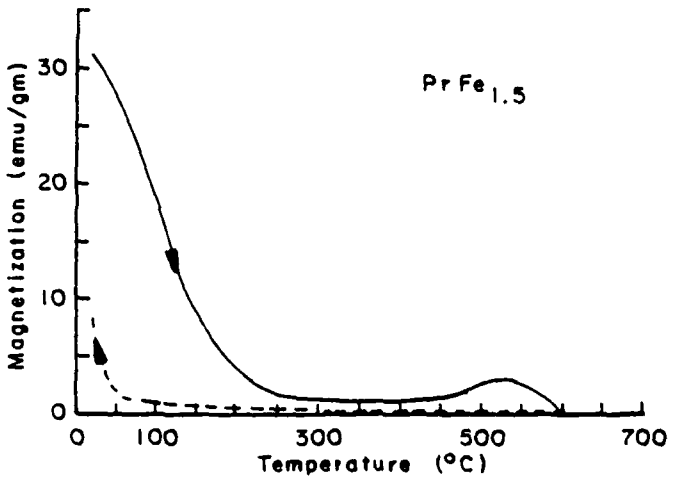

Figure 17. Magnetization variation with temperature for melt spun $PrFe_{1.5}$. The arrows indicate the data obtained during heating and cooling.

During heating, a magnetic transition at 230°C and the recrystallization hump near 500°C was observed. On cooling the alloy, it was found that only the 2:17 phase was present. This suggested the metastable alloy formed during quench when crystallized decomposes to 2:17 phase and possibly Pr. Similar observation has been reported by Croat[8]. The coercivity of the $PrFe_{1.5}$ phase was 250 Oe in the melt spun condition (see Table 7).

TABLE 7

MAGNETIC PROPERTIES OF R-Fe AND R-Fe-B
MELT SPUN ALLOYS

(Data collected on -35 mesh powder dispersed in plastic)

Alloy	H_{ci} (Oe)	
	As-Spun	Heat Treated
$PrFe_2$	1,300	0
$PrFe_{1.5}$	250	0
$PrFe_{1.25}B_{.25}$	25,900	15,300
$PrFe_{1.0}B_{0.5}$	3,500	28,200
$NdFe_{1.25}B_{0.25}$	22,600	21,600
$NdFe_{1.0}B_{0.5}$	26,000	26,800
$SmFe_{1.5}$	1,500	470
$SmFe_{1.25}B_{0.25}$	1,300	680
$SmFeB_{0.5}$	1,100	600
$PrFe_4B$	12,900	26,600
$PrFe_{6.4}B$	7,100	6,400
$NdFe_{6.4}B$	4,500	7,600

Pr-Y-Fe Alloys

In order to stabilize the magnetic phase, yttrium was substituted for Pr and boron for iron. The addition of yttrium was tried because a stable Laves phase YFe_2 has been reported and it was hoped small amounts of boron would help in stabilizing metastable phases. Light elements such as carbon and boron are known to stabilize magnetic phases such as Mn_5Si_3[9], MnAl[10], etc.

Three alloys were made in the $(PrY)Fe_2$ type with various yttrium substitutions for Pr.

Listed in Table 8 are the Curie temperatures, saturation magnetization and intrinsic coercive forces of $(PrY)Fe_2$ alloys.

TABLE 8

CURIE TEMPERATURES, SATURATION MAGNETIZATIONS AND INTRINSIC COERCIVE FORCES OF $(PrY)Fe_2$ ALLOYS

Alloys	Curie Temperature (T_c 1°C)	Saturation Magnetization σ(emu/gm)	Intrinsic Coercive Force (As-Spun) H_{ci} (Oe)
$PrFe_2$	21, 227, 575	44.2	1,300
$Pr_{0.7}Y_{0.3}Fe_2$	62	71.1	750
$Pr_{0.5}Y_{0.5}Fe_2$	147	68.3	350
$Pr_{0.3}Y_{0.7}Fe_2$	226	74.3	200

As shown in Table 8, the addition of yttrium increases the saturation magnetization of $PrFe_2$, but it does not have any improvement on the coercive force. The magnetic transition temperature increases as the yttrium content increases.

Pr-Fe-B Alloys

In order to stabilize the magnetic phase with a T_c of 230°C, boron was added to the $PrFe_{1.5}$. The M vs T data for $PrFe_{1.25}B_{0.25}$ and $PrFeB_{0.5}$ are shown in Figure 18.

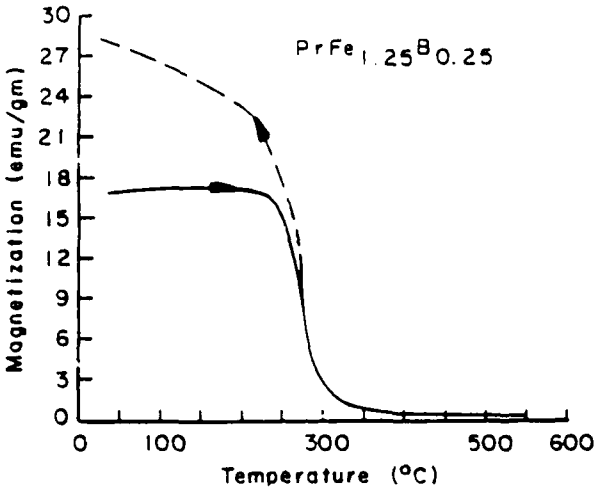

(a)

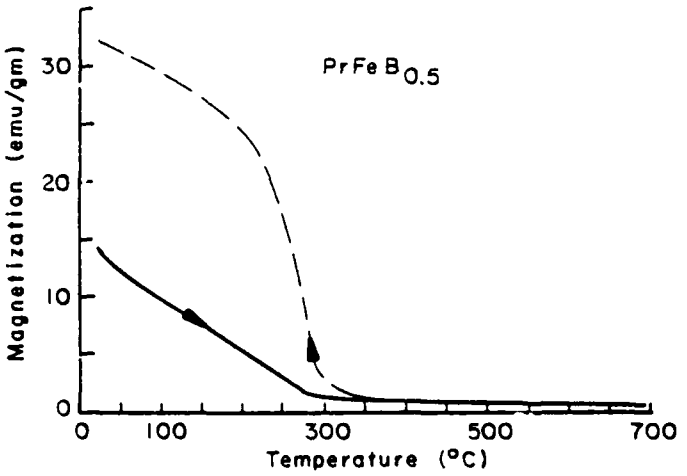

(b)

Figure 18. Magnetization variation with temperature for boron substituted $PrFe_{1.5}$ melt spun alloys.

A single-phase alloy with Curie temperature of 297°C was obtained. This phase appeared stable on heating and cooling. The coercivity observed were remarkably high. The X-ray diffraction on the as-spun and crystallized alloy did not correspond to the RFe_2 Laves phase (Figure 19). Simulated X-ray lines for the various rare earth-iron binary alloys are given in Appendix I.

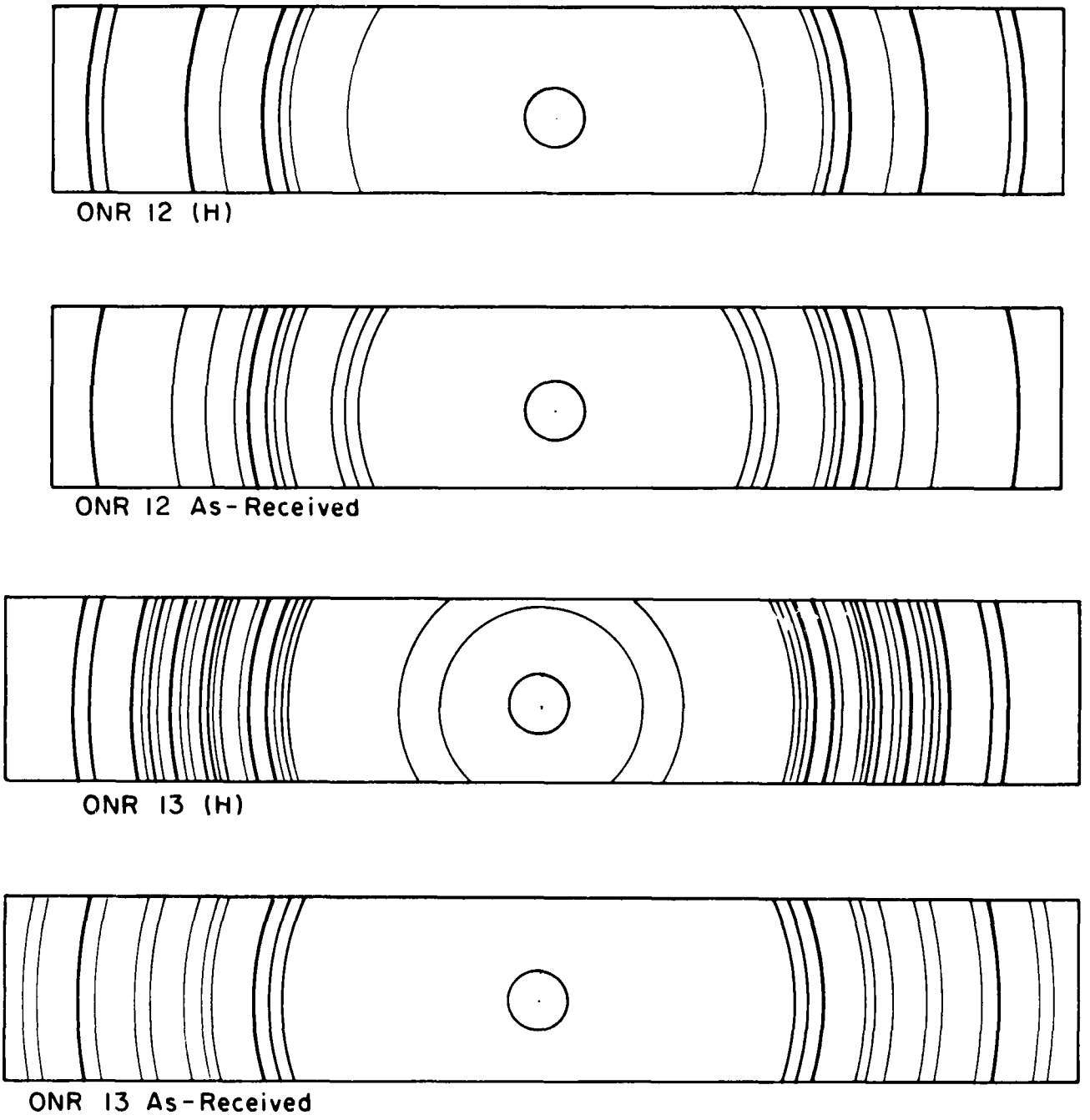

Figure 19. X-ray diffraction pattern on Pr-Fe alloys with boron addition. (H) refers to heat treated 700°C - 1 hr. ONR 12 = $PrFeB_{0.5}$, ONR 13 = $PrFe_{1.25}B_{0.25}$.

(Refer to Appendix I)

In order to increase the iron content further, an alloy $PrFe_4B$ was made and its M vs T characteristics are shown in Figure 20.

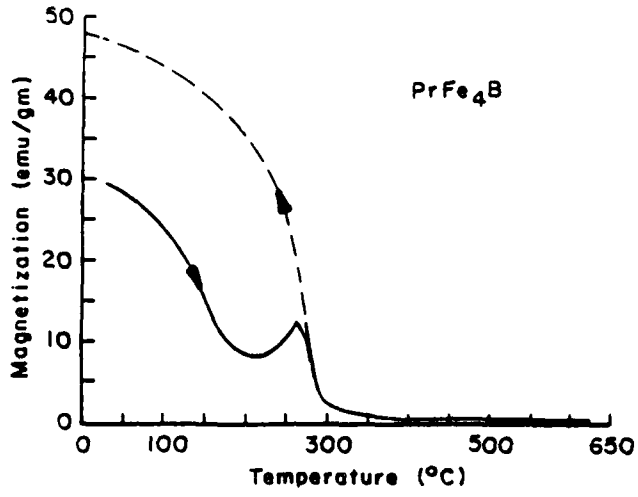

Figure 20. Magnetization variation with temperature for $PrFe_4B$ melt spun alloy.

The Curie temperature of this alloy was also 297°C and the intrinsic coercive force was still remarkably high (Table 7).

X-ray diffraction of the $PrFe_4B$ as melt spun and recrystallized are shown in Figure 21.

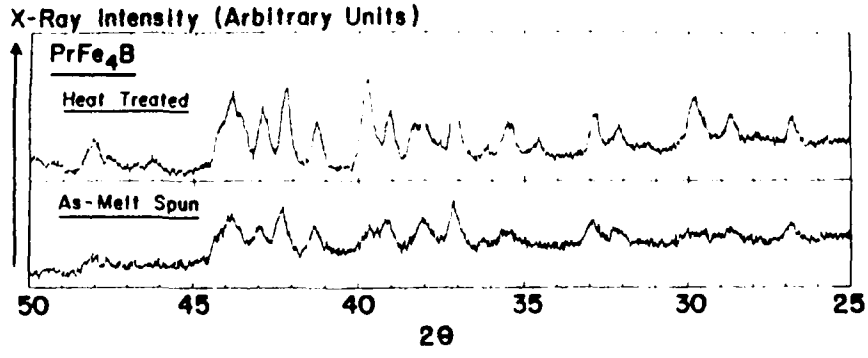

Figure 21. X-ray diffraction data collected using Cu k_α radiation for $PrFe_4B$ alloy melt spun and heat treated.

As can be seen, the heat treatment of the melt spun alloys improves the intensity of the lines but no new phase is formed during the heating process.

Pr-Fe-B-Si Alloys

Attempts were made to optimize the magnetic properties of the Pr-Fe alloys by varying the chemical composition to higher Fe concentrations to get higher magnetic moments[11]. The following two master alloys were vacuum melted:

Code	Master Alloy	Weight Percentage Pr	Fe	B	Wt. % Si
CRT-1A	$PrFe_{4.4}B_{0.26}Si_{0.18}$	38.7	67.15	0.77	1.38
CRT-1B	$PrFe_{7.5}B_{0.41}Si_{0.28}$	24.7	73.15	0.77	1.38

These alloys were blended in various proportions to vary the Pr content from 24.7% to 38.7% to optimize the magnetic characteristics. The blended alloys were remelted to assure the desired mixture prior to the melt spinning process.

The X-ray diffraction patterns on the as-melt spun CRT-1 and CRT-2 are shown in Figures 22 and 23. Also shown in the figure are the attempts to crystallize the ribbons by holding them at various temperatures. CRT-1 as-melt spun was amorphous whereas CRT-2 was crystalline. CRT-1 alloy crystallizes between 600 and 700°C.

Both the as-spun and crystallized alloys were first crushed to powder size of -35 mesh and dispersed in wax in a d. c. magnetic field for aligning the powder in the preferred magnetization direction. Intrinsic coercivity and remanence to saturation B_r/B_s ratio were measured. Table 9 lists the blended alloys and their H_{ci} and B_r/B_s ratios.

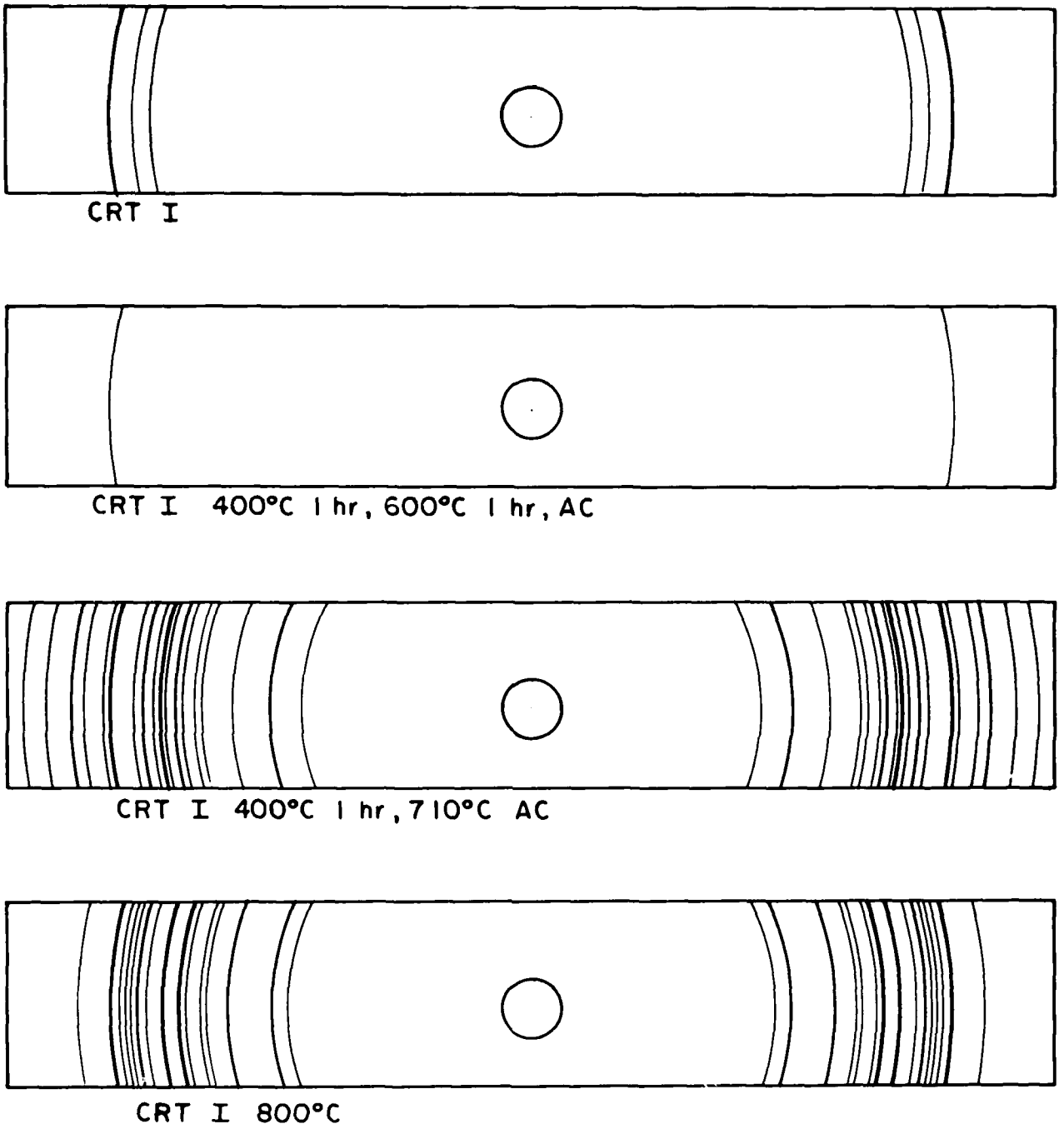

Figure 22. X-ray diffraction pattern of CRT-1 alloy heat treated at various temperatures.

(Refer to Appendix I)

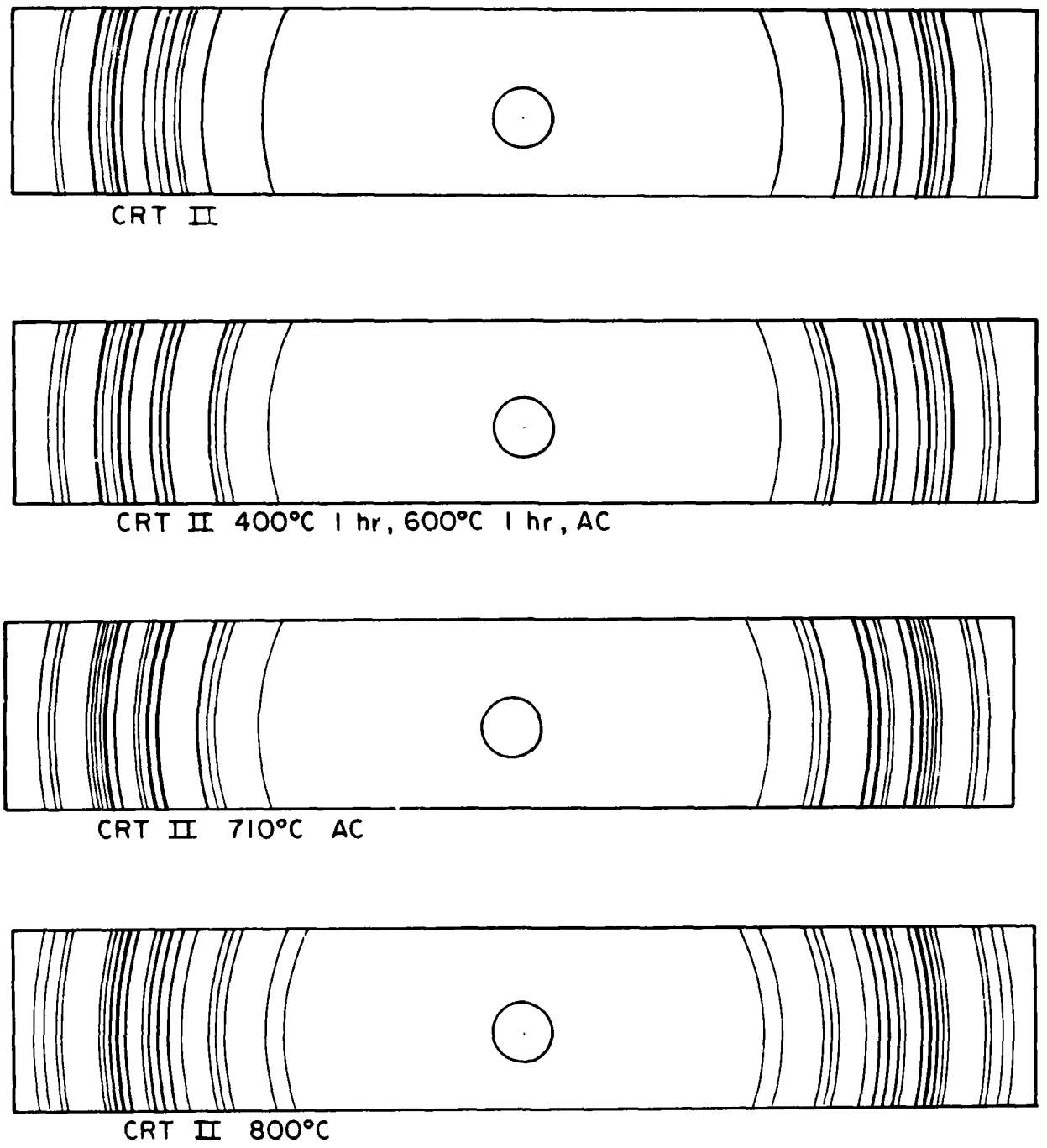

Figure 23. X-ray diffraction pattern of CRT-2 alloy heat treated at various temperatures.

(Refer to Appendix I)

TABLE 9

INTRINSIC COERCIVITY (H_{ci}) AND REMANENCE TO SATURATION (B_r/B_s) RATIO OF PrFeB Si ALLOYS

Alloys CRT-1A	Alloys CRT-1B	H_{ci} (Oe)		B_r/B_s	
Wt. %		As-Spun	Crystallized	As-Spun	Crystallized
100	0	11,500	11,100	0.55	0.62
80	20	9,000	7,750	0.54	0.64
60	40	5,800	7,200	0.52	0.61
50	50	4,800	5,500	0.48	0.56
40	60	580	620	0.23	0.29
20	80	1,800	2,900	0.41	0.55
0	100	490	1,000	0.21	0.32

As shown in Table 9, both H_{ci} and B_r/B_s decreases when CRT-1A content decreases. It indicates that CRT-1A has the favorable magnetic phase. Similar to $PrFe_4B$ or $PrFe_{6.4}B$, the M vs T data of CRT-1A (Figure 24) shows a maximum magnetization close to Curie temperature during heating. This maximum is attributed to the changes in the magnetic hardness of the material.

The M vs T data of CRT-1B shows that this alloy has a two-phase composition. According to the results of H_{ci} and B_r/B_s ratio, this two-phase alloy does not provide high values of H_{ci}.

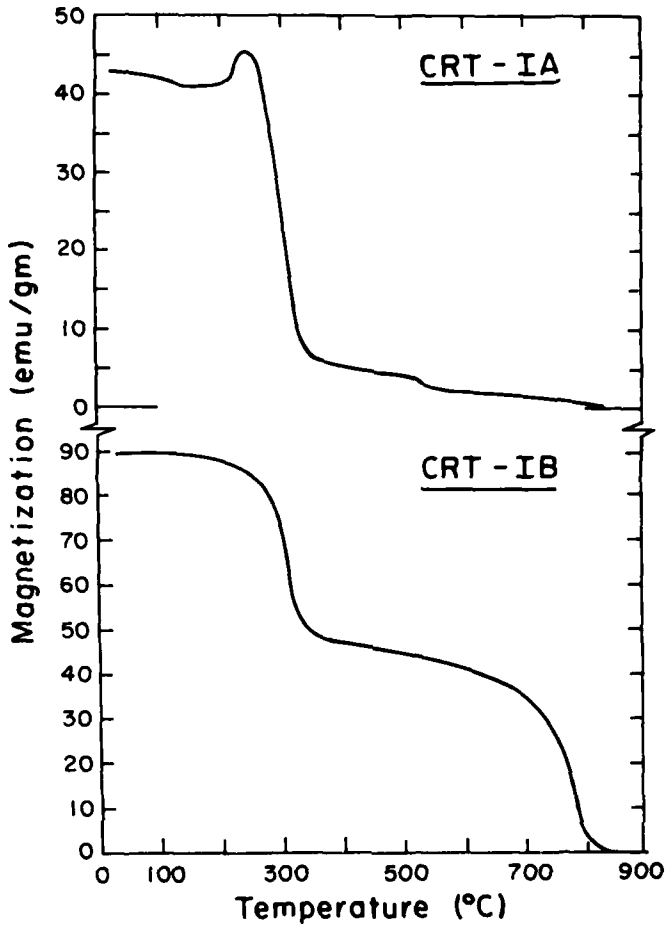

Figure 24. Magnetization vs Temperature of CRT-1A and CRT-1B.

Nd-Fe Alloys

Having observed high values of coercivity in the PrFeB alloys, we extended our investigation to the other rare earth alloys. Boron addition to Nd-Fe alloys proved beneficial as well. Intrinsic coercivity as 26,800 Oe was realized (Table 7).

The magnetization versus temperature data for the Nd-Fe alloys containing boron are shown in Figure 25.

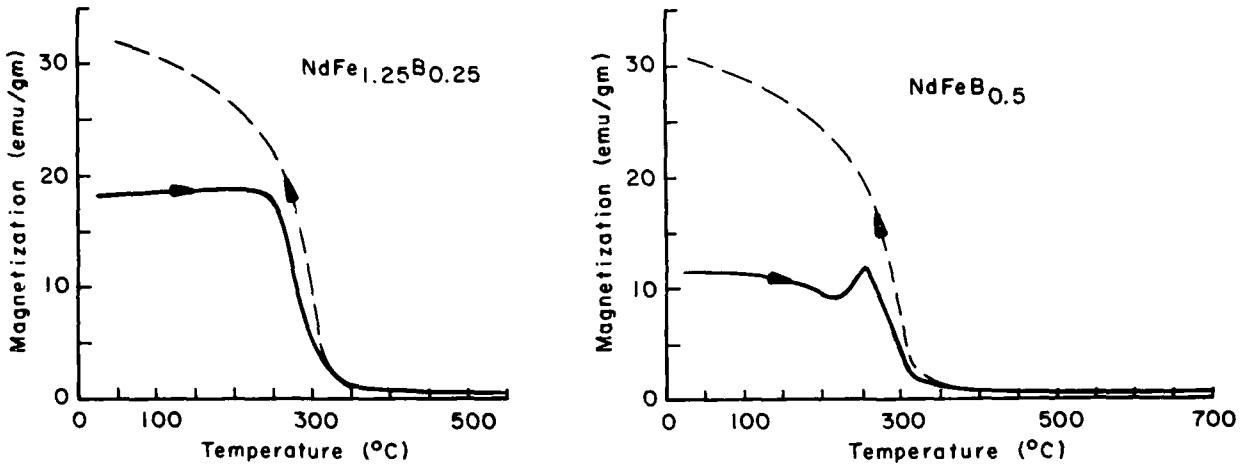

Figure 25. Magnetization vs Temperature data on Nd-Fe-B alloys.

The maximum in the magnetization observed close to the Curie temperature is attributed to the changes in the magnetic hardness of the material possibly because of changes in the Nd sublattice anisotropy. The increase in magnetization on cooling is due to the effect of magnetic field permitting the loose powder to orient more effectively at the Curie temperature.

The Curie temperature of the magnetic alloy is also around 300°C suggesting that the magnetic phase in the Nd-Fe system is similar to that observed in the Pr-Fe-B and Pr-Fe-B-Si alloys.

Sm-Fe Alloys

Sm-Fe alloys were also prepared by melt spinning. Magnetization versus temperature data indicate that as-melt spun alloys (Figure 26) have a magnetic transition temperature around 300°C but this phase is absent when the ribbons are taken to 600°C. After heating to 600°C and cooling, the Curie temperature of 400°C corresponds to that of $SmFe_2$. This suggests that the 300°C magnetic phase is unstable at 600°C. It is interesting to note that the $SmFe_2$, which is difficult to prepare in the conventional vacuum melting practices, can be prepared more easily by heat treating melt spun alloy. This has a high technological significance as $SmFe_2$ has high values for magnetostriction.

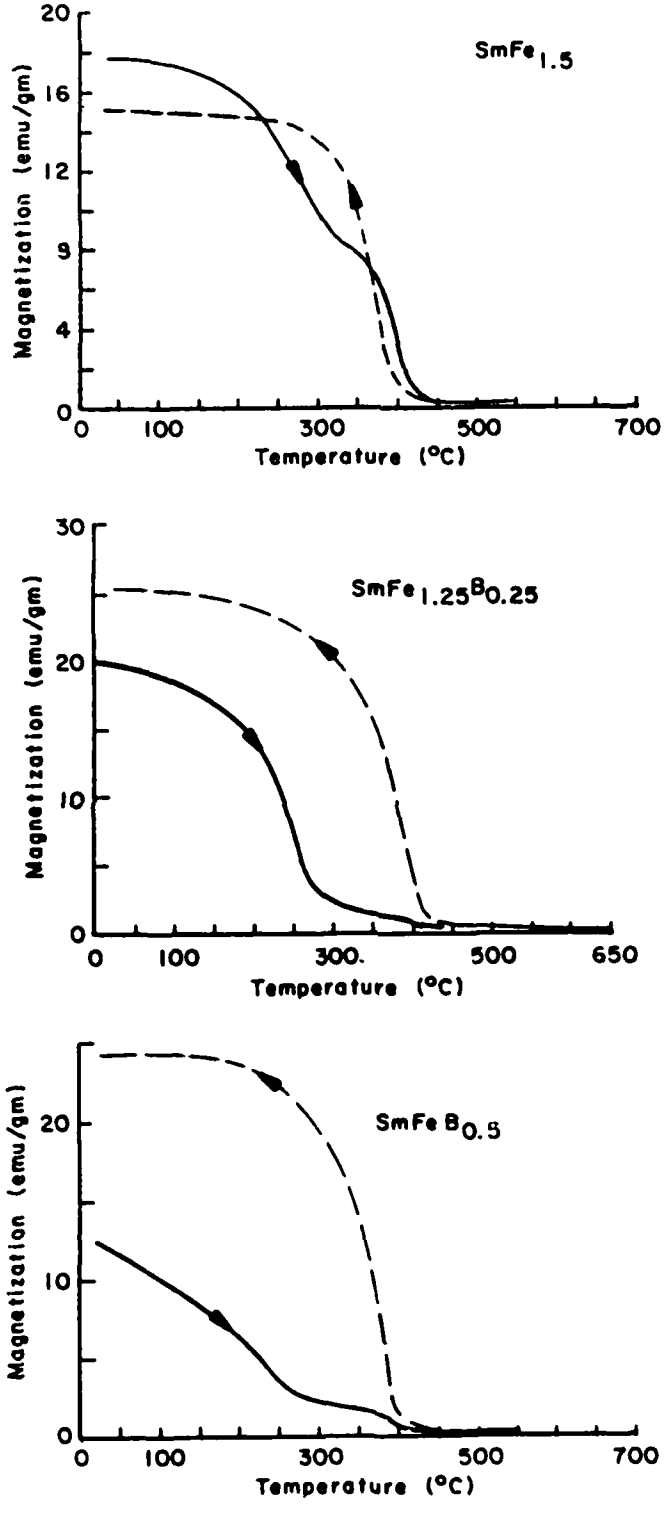

Figure 26. Magnetization versus Temperature for Sm-Fe and SmFeB alloys.

Magnetic Phase with a T_c ~300°C

Both the Pr-Fe, Nd-Fe and Sm-Fe alloys containing boron exhibited a Curie temperature near 300°C. Stadelmaier identified this phase to be of the composition $R_3Fe_{16}B$ or $R_3Fe_{20}B$. X-ray diffraction pattern of as-melt spun alloy of $NdFe_{6.4}B$ and $PrFe_{6.4}B$ is shown in Figure 27.

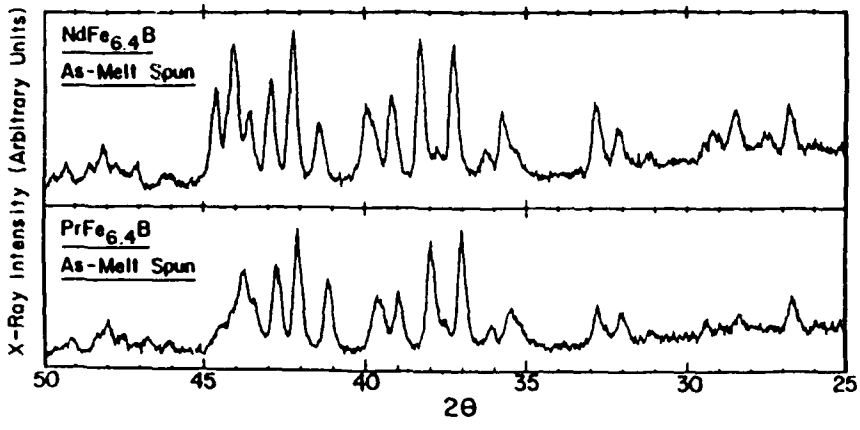

Figure 27. X-ray diffraction data on melt spun $PrFe_{6.4}B$ and $NdFe_{6.4}B$ alloys.

Indexing of the alloy to the tetragonal structure was possible and Table 10 provides hkl values. Lattice constants were: $a = 8.815$ Å and $c = 12.178$ Å.

Magnetization versus temperature data is shown for these two alloys in Figure 28. As can be seen from Figures 20, 24 and 28, the magnetic phase in all these alloys of Pr-Fe have the same Curie temperature. X-ray data comparison between Figure 21 and Figure 27 indicates that the magnetic phase in $PrFe_4B$ has nearly the same structure as $PrFe_{6.4}B$.

TABLE 10

X-RAY DATA ON $PrFe_{6.4}B$

hkℓ	I/I_o	d Spacing
212	W	3.338
220	VVW	3.133
114	VVW	2.797
311	W	2.730
312 204	W	2.528
223	VW	2.488
005 214	VS	2.429
105	S	2.370
313	W	2.309
115	W	2.270
224	W	2.196
410	S	2.146
411	W	2.115
330	W	2.071
314	VVW	1.970
331	VVW	1.943(?) 1.914(?)
413	VVW	1.897
206	VVW	1.855
?	W	1.715 ?
?	W	1.712 ?
207	W	1.620
335	W	1.595
513	VW	1.583
441	W	1.532
008	W	1.509
317	W	1.483
208	VVW	1.444
505 345	VW	1.430
533 515	VW	1.415
444	VW	1.391
228	VW	1.357
604	VW	1.321

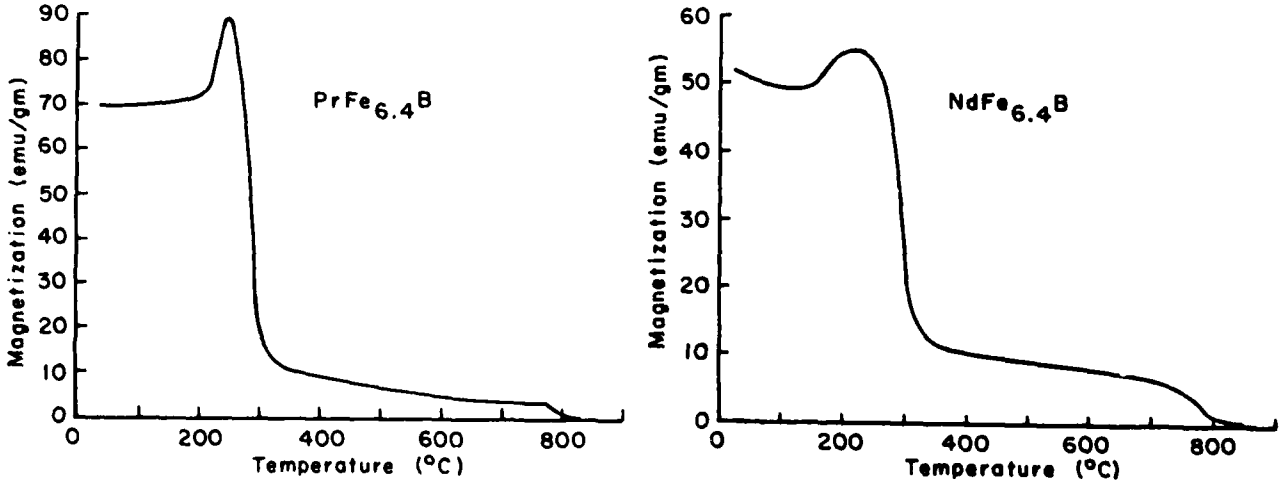

Figure 28. Magnetization versus temperature for NdFe melt spun alloys.

We made a series of alloys close to this composition. Anisotropy fields and saturation magnetizations were measured on the as-cast alloy. Anisotropy field was used as an indication for the potential to achieve coercivity. The magnetization on a powder pressed magnet will be considerably higher than that measured on an as-cast piece because of a better orientation of magnetic domains in the powder. Nevertheless, the as-cast alloys provide a fast indication of the potential of the alloys. Table 11 lists the anisotropy field and saturation magnetization measured on the as-cast $R_3T_{20}B$ alloys.

TABLE 11

ANISOTROPY FIELDS AND SATURATION MAGNETIZATION OF THE AS-CAST $R_3T_{20}B$ ALLOYS

Alloy	H_A kOe	$4\pi M_s$ (Gauss)
*$NdFe_7B_{0.33}$	47	11,900
*$NdFe_6NiB_{0.33}$	21	11,300
*$NdFe_{6.66}B_{0.33}$	52	11,600
$NdFe_{5.66}N_5B_{0.33}$	20	10,900
*$NdFe_{6.66}B$	46	9,750
$NdFe_{6.4}B$	52	8,700
*$NdFe_6Ni_{0.4}B$	60	10,800
*$NdFe_{5.4}NiB$	41	11,000
$NdFe_{4.4}Ni_2B$	-	9,300

*Alloys were selected for melt spinning.

Alloys with high saturation magnetization and high anisotropy field were selected for the melt spinning process. Intrinsic coercivity H_{ci} and B_r/B_s ratio were measured in the as-spun and crystallized states. Table 12 shows the H_{ci}, B_r/B_s and Curie temperature of melt spun $R_3T_{20}B$ alloys.

TABLE 12

INTRINSIC COERCIVITY H_{ci}, REMANENCE TO SATURATION RATIO B_r/B_s AND THE CURIE TEMPERATURE OF MELT SPUN $R_3T_{20}B$ ALLOYS IN THE AS-SPUN AND CRYSTALLIZED STATES

Alloys	H_{ci} (Oe)		B_r/B_s		T_c (°C)
	As-Spun	Crystallized	As-Spun	Crystallized	
$NdFe_7B_{0.33}$	1,600	1,400	0.36	0.36	299, 784
$NdFe_6NiB_{0.33}$	200	400	0.09	0.20	358, 788
$NdFe_{6.66}B_{0.33}$	1,600	1,900	0.39	0.46	304
$NdFe_{6.66}B$	2,950	1,900	0.44	0.41	295, 784
$NdFe_6Ni_{0.4}B$	5,500	4,000	0.51	0.54	345
$NdFe_{5.4}NiB$	1,300	4,100	0.34	0.52	260, 346, 487, 784

The addition of Ni increases the Curie temperature of hard magnetic phase. With the Ni addition, higher metalloid content appears to be required to maintain the coercivity

The M vs T data of $R_3T_{20}B$ melt spun alloy during heating are shown in Figure 29.

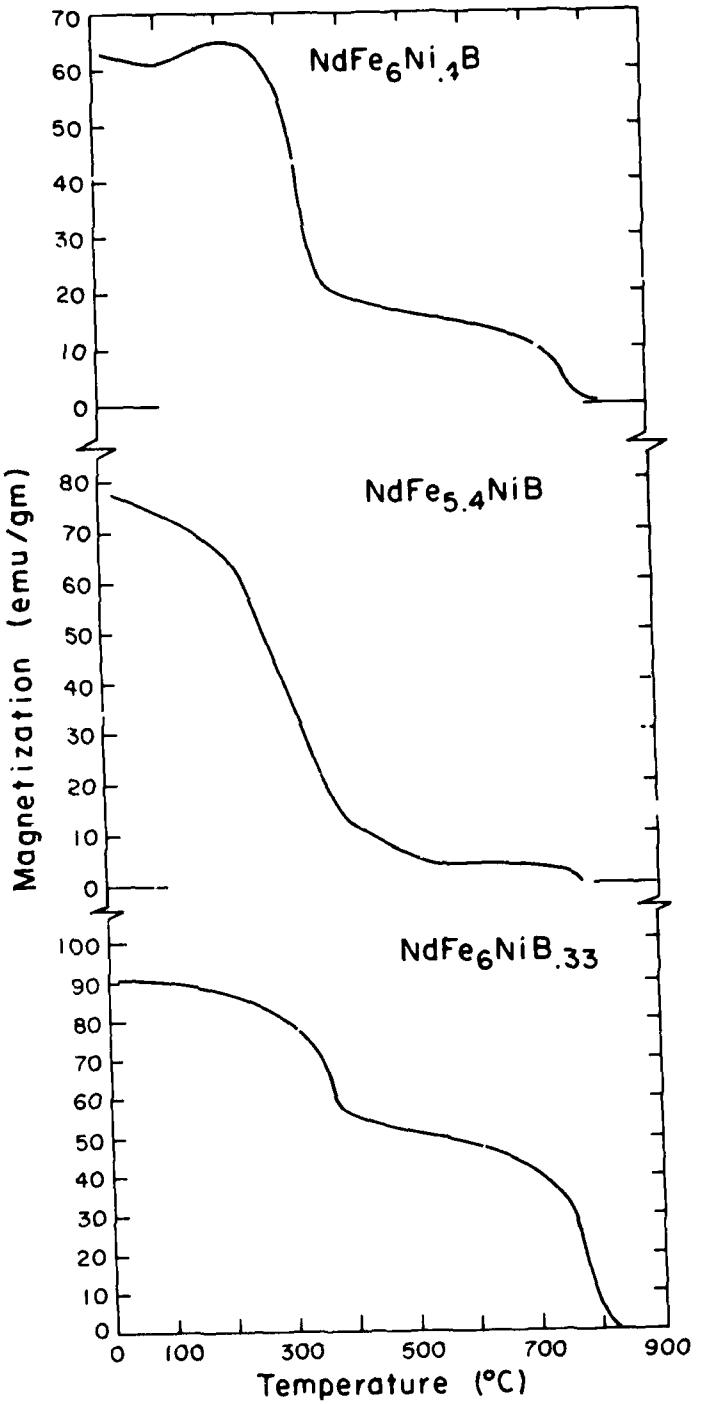

Figure 29. Magnetization versus temperature of nickel containing Nd-Fe melt spun alloys.

SECTION 5

CONCLUSIONS

The objective of the ONR program was to develop alloy compositions that can be fabricated into magnets using raw materials that are not of strategic importance.

We have successfully identified a series of alloys that have high saturation induction and coercive force. Exploitation of these alloys for permanent magnet manufacture will be useful.

Specifically NdFeB and PrFeB alloys, with a composition of $R_3T_{20}B$ and $R_3T_{16}B$ have been identified as useful alloys.

Future work on the higher iron containing alloys will be useful for the development of an iron permanent magnet with perhaps very little or no rare earth.

SECTION 6

REFERENCES

1. G. Y. Chin, S. Sibler, J. C. Belts, T. D. Sclabath, F. E. Werner, and D. L. Martin, "Impact of Recent Cobalt Supply Situation on Magnetic Materials and Applications" IEEE, Trans. Magn., Vol - MAG15, 1979, p. 1685.

2. N. C. Koon, C. M. Williams and B. N. Das, "A New Class of Melt-Quenched Amorphous Alloys" International Conf. on Magnetism and Magnetic Materials, Dallas, 1980.

3. A. E. Clark, "Magnetic and Magneto Elastic Properties of Highly Magnetostrictive Rare Earth-Iron Laves Phase Compounds," AIP Conf., Proc. No. 18, Pt. 2, 1973, p. 1015.

4. J. Schweizer, "Review of the Structures and Properties of the Rare Earth-Iron Compounds of Formula R_2Fe_{17}" AFML-TR-71-36, p. 30.

5. K. H. J. Buschow, "Intermetallic Compounds of Rare Earth and 3d Transition Metals," Rep. Prog. Phys., 40, 1977, p. 1179.

6. P. C. M. Gubbens, "Magnetic Properties of Rare Earth-Iron Compounds," PH.D. these (Delft Univ. Press) (Amsterdam), 1977.

7. K. S. V. L. Narasimhan and W. E. Wallace, "Magnetic Properties of R_2Fe_{17} M (R=Y, Tm, Ho and M=Ni, Al) and Y_2-Y $ThyFe_{17}$ Compounds," AIP Conf. Proc. No. 18, Pt., 1973, p. 1248.

8. J. J. Croat, "Magnetic Properties of Spun Melt Praseodymium-Iron Alloys," J. App. Phys. 52, 2509, 1981.

K. H. J. Buschow, "On the Crystallization Behavior of Amorphous Alloys of Rare Earths and 3d Transition Metals," J. Phys. D: App. Phys., 13, 251, 1980.

K. H. J. Buschow, "Crystallization and Magnetic Properties of Amorphous Gd-Fe and Er-Fe Alloys," J. Less. Comm. Metals, 66, 89, 1979.

9. Y. Lecocq, P. Lecocq, and A. C. Michel, r. Acad. Sci. Paris, 258, 5655, 1964.

10. S. Kojima, T. Ohtani, N. Kato, K. Kojima, Y. Sakamoto, I. Konno, M. Tsukahara and T. Kubo, "Crystal Transformation and Orientation of Mn-Al-C Hard Magnetic Alloy," AIP Conf. Proc., No. 24, pp. 768-769, 1974.

11. G. C. Hadjipanayis, R. C. Hazelton, and K. R. Lawless, Applied Physics Letters 43, 797, 1983.

APPENDIX I

X-ray Data on R-Fe Phases

X-ray diffraction data on the alloys made by the melt spun process are shown in Figures 19, 22 and 23. Since a variety of phases can be formed between the rare earth and the iron, a simulated X-ray diffraction pattern for RFe_2, R_2Fe_{17} (hexagonal), R_2Fe_{17} (rhombohedral), and the new magnetic phase $RFe_{6.4}B$ are shown on Pages A-1, A-2, A-3 and A-4 respectively. Superposition of these patterns on top of any of the data collected can provide clues to the phases that are present.

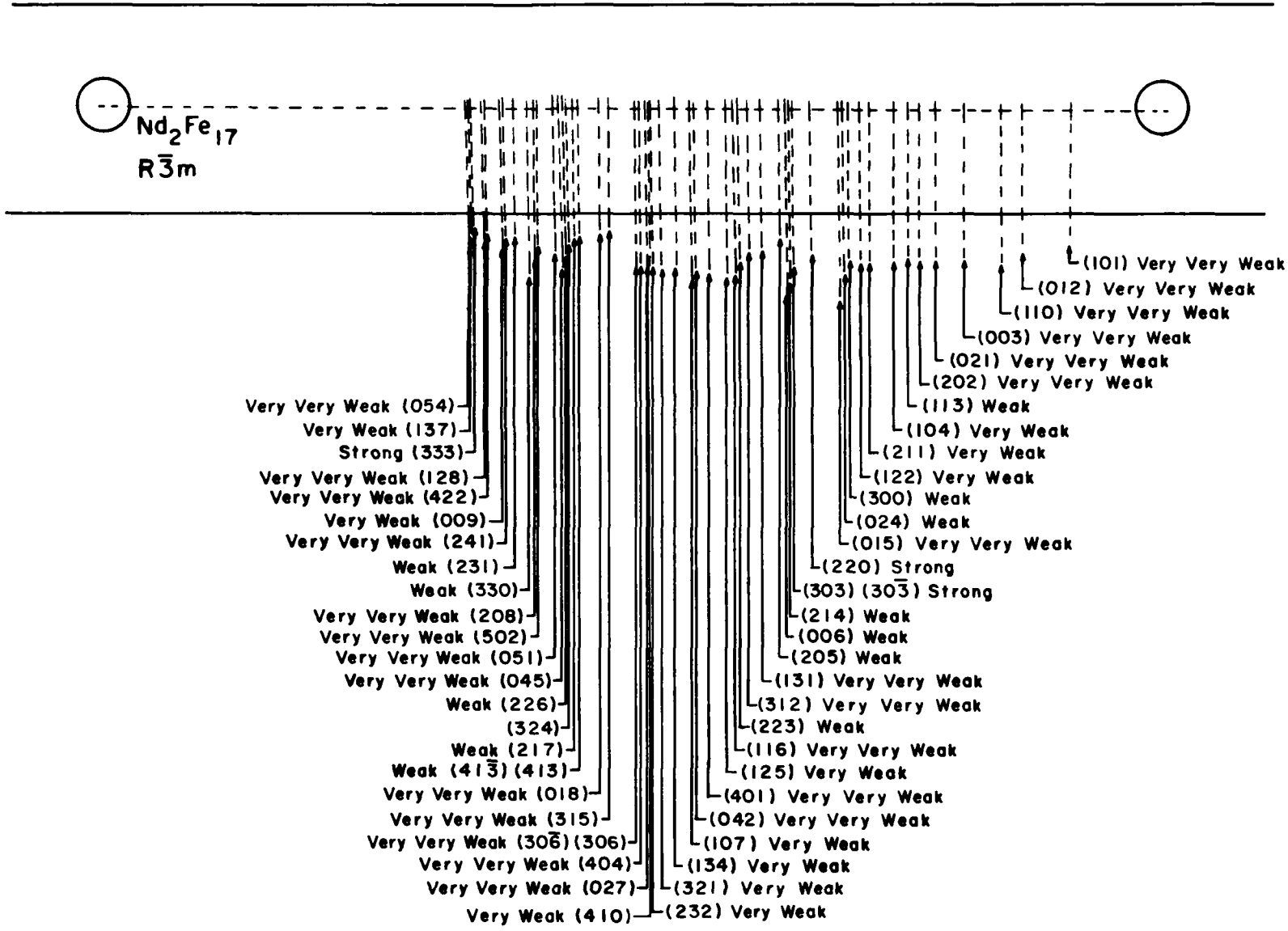
Nd_2Fe_{17}
$R\bar{3}m$
Very Very Weak (054)
Very Weak (137)
Strong (333)
Very Very Weak (128)
Very Very Weak (422)
Very Weak (009)
Very Very Weak (241)
Weak (231)
Weak (330)
Very Very Weak (208)
Very Very Weak (502)
Very Very Weak (051)
Very Very Weak (045)
Weak (226)
(324)
Weak (217)
Weak ($41\bar{3}$) (413)
Very Very Weak (018)
Very Very Weak (315)
Very Very Weak ($30\bar{6}$) (306)
Very Very Weak (404)
Very Very Weak (027)
Very Weak (410)
(232) Very Weak
(321) Very Weak
(134) Very Weak
(107) Very Weak
(042) Very Very Weak
(401) Very Very Weak
(125) Very Weak
(116) Very Very Weak
(223) Weak
(312) Very Very Weak
(131) Very Very Weak
(205) Weak
(006) Weak
(214) Weak
(303) ($30\bar{3}$) Strong
(220) Strong
(015) Very Very Weak
(024) Weak
(300) Weak
(122) Very Weak
(211) Very Weak
(104) Very Weak
(113) Weak
(202) Very Very Weak
(021) Very Very Weak
(003) Very Very Weak
(110) Very Very Weak
(012) Very Very Weak
(101) Very Very Weak

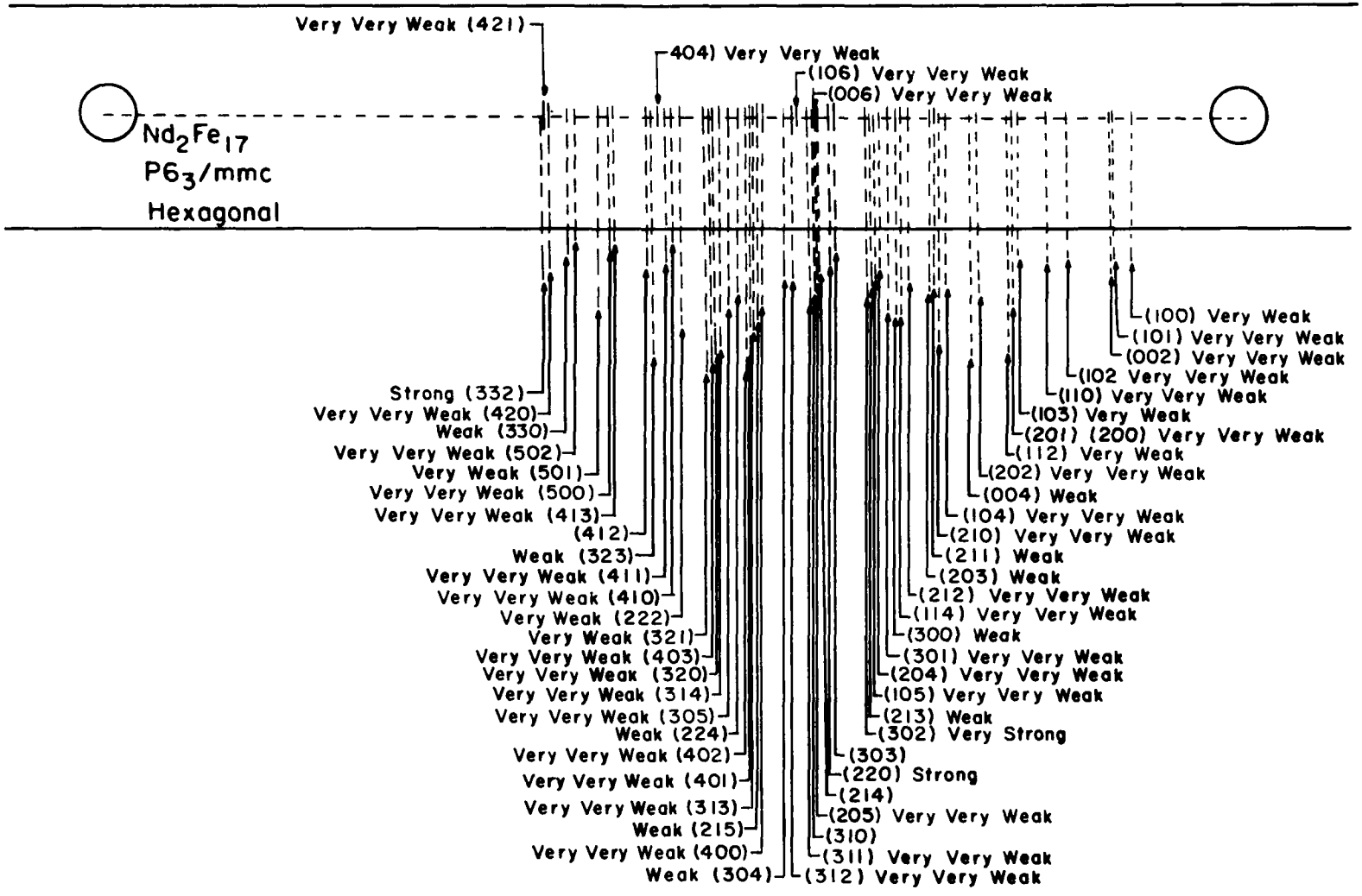
Nd2Fe17
P63/mmc
Hexagonal
Very Very Weak (421)
404) Very Very Weak
(106) Very Very Weak
(006) Very Very Weak
(100) Very Weak
(101) Very Very Weak
(002) Very Very Weak
(102 Very Very Weak
(110) Very Very Weak
(103) Very Weak
(201) (200) Very Very Weak
(112) Very Weak
(202) Very Very Weak
(004) Weak
(104) Very Very Weak
(210) Very Very Weak
(211) Weak
(203) Weak
(212) Very Very Weak
(114) Very Very Weak
(300) Weak
(301) Very Very Weak
(204) Very Very Weak
(105) Very Very Weak
(213) Weak
(302) Very Strong
(303)
(220) Strong
(214)
(205) Very Very Weak
(310)
(311) Very Very Weak
(312) Very Very Weak
Strong (332)
Very Very Weak (420)
Weak (330)
Very Very Weak (502)
Very Weak (501)
Very Very Weak (500)
Very Very Weak (413)
(412)
Weak (323)
Very Very Weak (411)
Very Very Weak (410)
Very Weak (222)
Very Weak (321)
Very Very Weak (403)
Very Very Weak (320)
Very Very Weak (314)
Very Very Weak (305)
Weak (224)
Very Very Weak (402)
Very Very Weak (401)
Very Very Weak (313)
Weak (215)
Very Very Weak (400)
Weak (304)

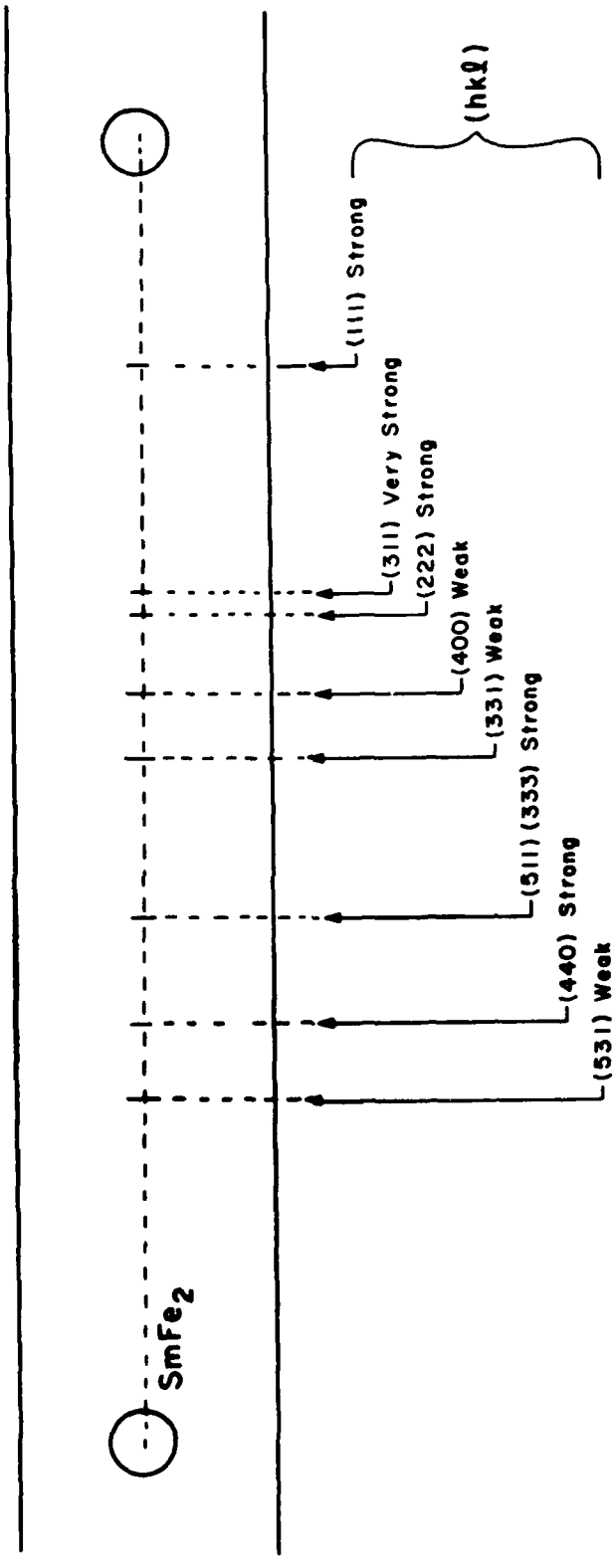
(hkl)
(111) Strong
(311) Very Strong
(222) Strong
(400) Weak
(331) Weak
(511) (333) Strong
(440) Strong
(531) Weak
SmFe2

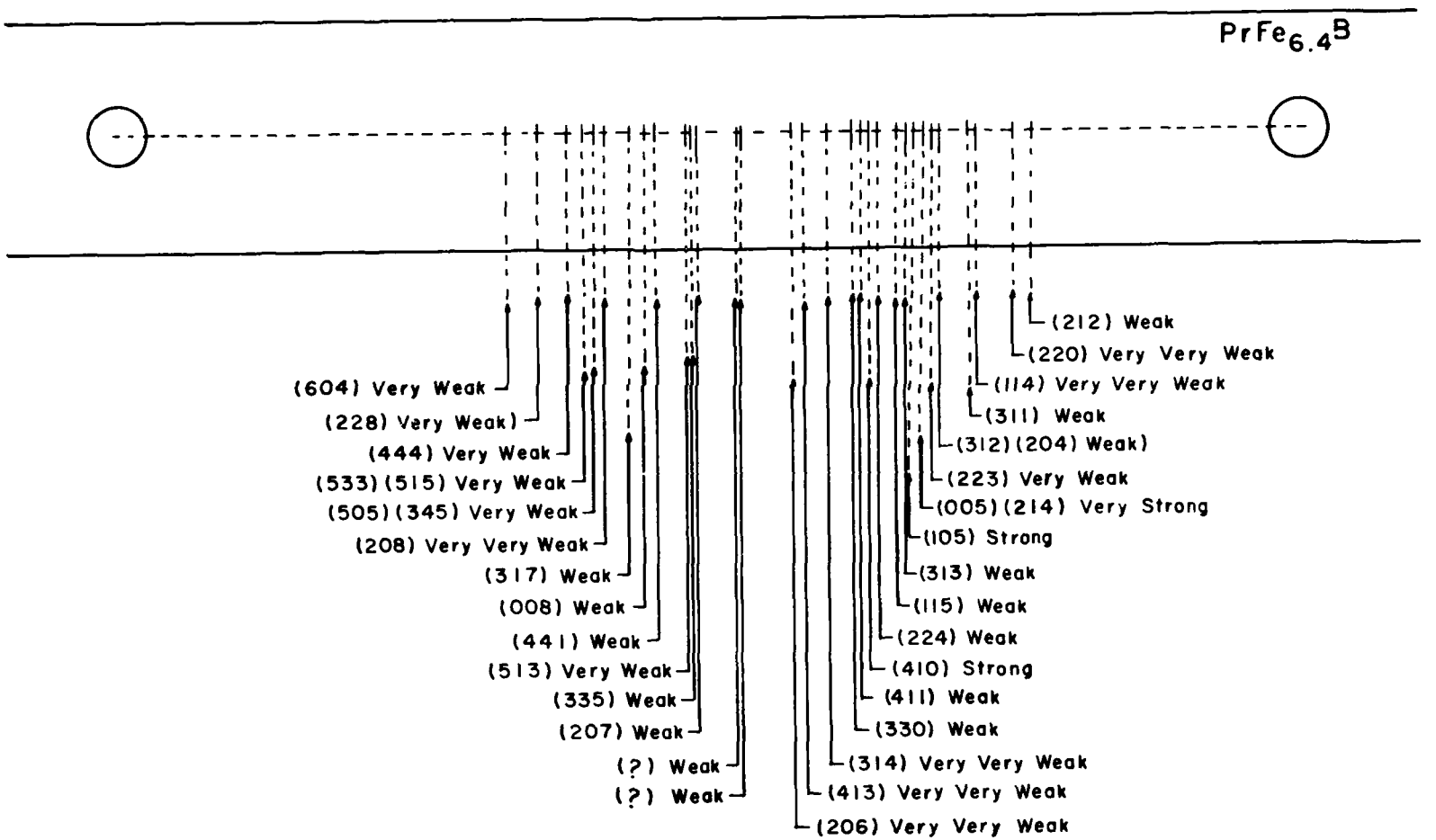
PrFe6.4B
(604) Very Weak
(228) Very Weak)
(444) Very Weak
(533) (515) Very Weak
(505) (345) Very Weak
(208) Very Very Weak
(317) Weak
(008) Weak
(441) Weak
(513) Very Weak
(335) Weak
(207) Weak
(?) Weak
(?) Weak
(206) Very Very Weak
(413) Very Very Weak
(314) Very Very Weak
(330) Weak
(411) Weak
(410) Strong
(224) Weak
(115) Weak
(313) Weak
(105) Strong
(005) (214) Very Strong
(223) Very Weak
(312) (204) Weak)
(311) Weak
(114) Very Very Weak
(220) Very Very Weak
(212) Weak

END

FILMED

2-85

DTIC